AD-A264 300

Diagnostics of Magnetic Substorms Using Satellite Observations of Magnetic Pulsations

FINAL REPORT

DTIC
ELECTE
MAY 1 4 1993
S **C** **D**

Prepared by

Chin S. Lin

for

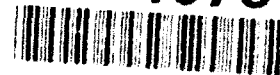Air Force Office of Scientific Research
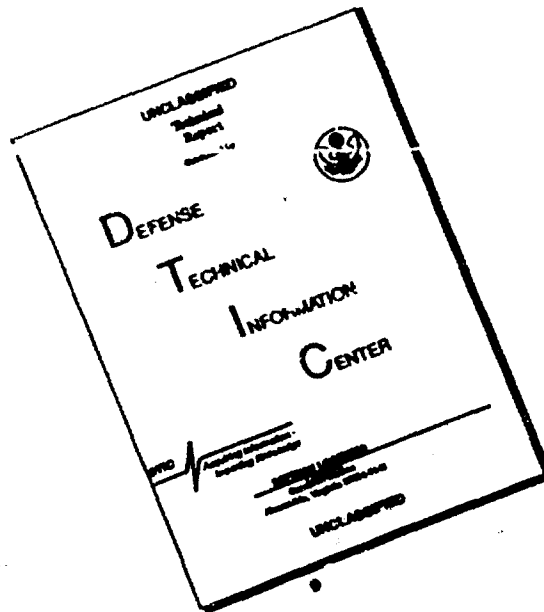Bolling Air Force Base, DC 20332-6448

26 October 1992
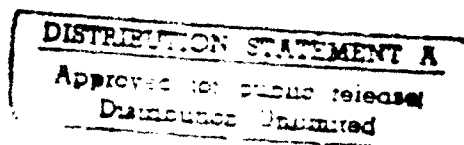
93-10754

93 5 13 051

DISCLAIMER NOTICE

THIS DOCUMENT IS BEST QUALITY AVAILABLE. THE COPY FURNISHED TO DTIC CONTAINED A SIGNIFICANT NUMBER OF PAGES WHICH DO NOT REPRODUCE LEGIBLY.

REPORT DOCUMENTATION PAGE

Form Approved
OMB No 0704-0188

1a. REPORT SECURITY CLASSIFICATION	1b. RESTRICTIVE MARKINGS
Unclassified	
2a. SECURITY CLASSIFICATION AUTHORITY	3. DISTRIBUTION/AVAILABILITY OF REPORT
2b. DECLASSIFICATION/DOWNGRADING SCHEDULE	Unlimited

4. PERFORMING ORGANIZATION REPORT NUMBER(S)	5. MONITORING ORGANIZATION REPORT NUMBER(S)

6a. NAME OF PERFORMING ORGANIZATION	6b. OFFICE SYMBOL (If applicable)	7a. NAME OF MONITORING ORGANIZATION
Southwest Research Institute	SwRI	APOSR/NL

6c. ADDRESS (City, State, and ZIP Code)	7b. ADDRESS (City, State, and ZIP Code)
P.O. Drawer 28510 San Antonio, TX 78228-0510	110 Duncan Ave. Suite B115 Bolling Air Force Base, DC 20332-0001

8a. NAME OF FUNDING/SPONSORING ORGANIZATION	8b. OFFICE SYMBOL (If applicable)	9. PROCUREMENT INSTRUMENT IDENTIFICATION NUMBER
of Scientific Research	APOSR/NL	F49620-89-C-0008

8c. ADDRESS (City, State, and ZIP Code)	10. SOURCE OF FUNDING NUMBERS			
110 Duncan Ave. Suite B115 Bolling Air Force Base, DC 20332-6448	PROGRAM ELEMENT NO	PROJECT NO	TASK NO	WORK UNIT ACCESSION NO
	61102F	2311	A1	

11. TITLE (Include Security Classification)
Diagnostics of Magnetic Substorms Using Satellite Observations of Magnetic Pulsations (Unclassified)

12. PERSONAL AUTHOR(S)
Dr Chin S. Lin

13a. TYPE OF REPORT	13b. TIME COVERED	14. DATE OF REPORT (Year, Month, Day)	15 PAGE COUNT
Final	FROM 10/1/88 TO 10/31/92	10-26-92	

16. SUPPLEMENTARY NOTATION

17	COSATI CODES		18. SUBJECT TERMS (Continue on reverse if necessary and identify by block number)
FIELD	GROUP	SUB-GROUP	

19. ABSTRACT (Continue on reverse if necessary and identify by block number)
This project has demonstrated that one class of magnetic pulsations known as stormtime Pc 5 waves is correlated with substorm onsets. Stormtime Pc 5 waves observed by geostationary satellites in the afternoon sector is characterized by oscillations of magnetic field with a period from 2 to 10 minutes, easily detected by magnetometers on communication or weather satellites. The estimated substorm onset times are found to be within 20 minutes of the actual substorm onset times. Geosynchronous satellites in the afternoon sector would detect these low frequency wave events about 2-4 hours after a substorm onset occurring at local midnight. The delay time depends on the propagation velocity, which varies from a few km/s up to 50 km/s. The disturbed region of a stormtime Pc 5 event has a longitudinal extent varying between 30 and 90 degrees. The study shows that stormtime Pc 5 waves have a wave amplitude confined with about $10°$ from the magnetic equator. The propagation velocity is found to increase with wave frequency and with the magnetic field inclination angle. Comparison of the statistical properties of stormtime Pc 5 waves with theoretical calculations of propagation velocity suggests that the propagation velocity of stormtime Pc 5 waves agrees better with the perpendicular group velocity of drift mirror mode. The propagation velocity of stormtime Pc 5 waves appears to be mainly determined by wave parallel wavelength, which is in turn determined by the inclination angle or the magnetic field topology. The obtained results about the propagation properties of magnetic pulsations during storm times is important for the satellite operation since it can be used to predict the plasma environment a synchronous satellite might encounter.

20. DISTRIBUTION/AVAILABILITY OF ABSTRACT	21. ABSTRACT SECURITY CLASSIFICATION
☒ UNCLASSIFIED/UNLIMITED ☐ SAME AS RPT ☐ DTIC USERS	Unclassified

22a. NAME OF RESPONSIBLE INDIVIDUAL	22b. TELEPHONE (Include Area Code)	22c. OFFICE SYMBOL
HENRY R. RADOSKI	(202) 767-5021	NL

DD Form 1473, JUN 86 · Previous editions are obsolete · SECURITY CLASSIFICATION OF THIS PAGE

3 NOV 1992

Diagnostics of Magnetic Substorms Using Satellite Observations of Magnetic Pulsations

FINAL REPORT

AFOSR Grant F49620-89-C-008
SwRI project No. 15-2570

Prepared by

Chin S. Lin

for

Air Force Office of Scientific Research
Bolling Air Force Base, DC 20332-6448

26 October 1992

Approved by

$\qquad\qquad$, 3

J. L. Burch

James L. Burch, Vice President
Instrumentation and Space Research

Abstract

This project has demonstrated that one class of magnetic pulsations known as stormtime Pc 5 waves is correlated with substorm onsets. Stormtime Pc 5 waves observed by geostationary satellites in the afternoon sector is characterized by oscillations of magnetic field with a period from 2 to 10 minutes, easily detected by magnetometers on communication or weather satellites. The estimated substorm onset times are found to be within 20 minutes of the actual substorm onset times. Geosynchronous satellites in the afternoon sector would detect these low frequency wave events about 2-4 hours after a substorm onset occurring at local midnight. The delay time depends on the propagation velocity, which varies from a few km/s up to 50 km/s. The disturbed region of a stormtime Pc 5 event has a longitudinal extent varying between 30 and 90 degrees. The study shows that stormtime Pc 5 waves have a wave amplitude confined with about 10° from the magnetic equator. The propagation velocity is found to increase with wave frequency and with the magnetic field inclination angle. Comparison of the statistical properties of stormtime Pc 5 waves with theoretical calculations of propagation velocity suggests that the propagation velocity of stormtime Pc 5 waves agrees better with the perpendicular group velocity of drift mirror mode. The propagation velocity of stormtime Pc 5 waves appears to be mainly determined by wave parallel wavelength, which is in turn determined by the inclination angle or the magnetic field topology. The obtained results about the propagation properties of magnetic pulsations during storm times is important for the satellite operation since it can be used to predict the plasma environment a synchronous satellite might encounter.

Table of Contents

I Introduction

This report summarizes the research findings obtained during the support of the Air Force Office of Scientific Research (AFOSR) grant F49620-89-C-0008. One objective of the grant is to investigate the feasibility of using dual satellite observations of low frequency magnetic pulsations to remotely diagnose substorm onsets. Another objective of the study is to understand the propagation velocity of stormtime Pc 5 waves, including its dependence on plasma variables and its correlation with physical parameters.

Synchronous satellites stationary over North America generally detected low frequency magnetic pulsation about 2-4 hours after substorm onsets occurring near local midnight over the Russian stations. In this project we investigated the feasibility of remotely sensing auroral substorm activities near midnight by using magnetic field measurements from synchronous satellites on the dayside. A synchronous satellite observing magnetic activities on the dayside is difficult to measure remotely auroral substorm activities occurring on the other side of Earth. The knowledge of substorm activities is important for the satellite operation since it can be used to predict the plasma environment a synchronous satellite might encounter. During auroral substorm activities, energetic plasma has been injected into the nightside magnetosphere, and precipitated into the ionosphere along magnetic field lines, producing auroras, ionospheric disturbance, and electromagnetic radiation over a wide frequency range. As a result, spacecraft are sometimes charged to a higher potential, affecting the operation.

GOES synchronous satellite magnetic field data since 1979 have been surveyed and statistically correlated with magnetograms from Russian ground stations in this project. It is found that one class of magnetic pulsations known as stormtime Pc 5 waves is correlated with substorm onsets. This class of magnetic pulsations is characterized by oscillations of magnetic field with a period from 2 to 10 minutes, easily detected by magnetometers on communication or weather satellites. Because these waves propagate from midnight to dayside after substorm onsets with high speed, they can be used to remotely diagnose substorm activities when geosynchronous satellites observe them on the dayside.

Figure 1 illustrates the schematic of determining the propagation velocity of magnetic pulsations from GOES magnetic field measurements. Two GOES satellites usually separated by two hours will detect the onset of a low frequency magnetic pulsation event within a period of 10-30 minutes. As shown in the schematic, the onset time at each GOES satellite is determined by the peak of the first oscillation. The propagation velocity is then calculated from the satellite separation distance D and the time difference Δt between the onset times observed by the two GOES satellites. Assuming a substorm onset near local midnight, the substorm onset time is estimated from the wave

1

propagation velocity and the distance S from local midnight to the satellite (Figure 1).

The results obtained in this study suggest that stormtime Pc 5 waves are correlated with substorm onsets. The estimated substorm onset times are found to be within 20 minutes of the actual substorm onset times. Geosynchronous satellites in the afternoon sector would detect these low frequency wave events about 2-4 hours after a substorm onset occurring at local midnight. The delay time depends on the propagation velocity, which varies from a few km/s up to 50 km/s. The propagation velocity is found to increase with wave frequency, which is found to be correlated with the magnetic field inclination angle. Comparison of the statistical properties of stormtime Pc 5 waves with theoretical calculations of propagation velocity supports that stormtime Pc5 waves propagate as the drift mirror mode. The propagation velocity of stormtime Pc 5 waves appears to be mainly determined by wave parallel wavelength, which is in turn determined by the inclination angle or the magnetic field topology.

Below we briefly summarize the results, and describe in detailed the analysis in the following sections.

A   Remote Diagnostic of Substorm Onsets

We conducted data analyses of GOES dual satellite magnetic field data for the years of 1979, 1983, and 1986. We investigated the correlation of stormtime Pc 5 waves with substorm onsets. From the data set, we selected stormtime Pc 5 events that ground station magnetometers were available. Because most correlated ground station magnetometer data were collected in Russia, we were able to conducted the correlation study only for the data set of 1979. We described the results in Section II.

This study used simultaneous observations of stormtime Pc 5 events by the GOES 2 and GOES 3 geostationary satellites to study the correlation of Pc 5 waves with substorm onsets. Eighteen Pc 5 events occurring from March to December 1979 were first surveyed. After excluding events with highly varying activity or scarce station coverage, only six events with clear substorm features 2-4 hours before the GOES observation of the Pc 5 events were then analyzed. From the wave propagation speed and the distance from local midnight to the satellite position, the substorm onset time was estimated. For the six events examined, ground magnetograms near local midnight indicate that a substorm onset occurred within 20 minutes of the estimated substorm onset times. This result suggests that the occurrence of stormtime Pc 5 waves is probably correlated with substorm onsets. The results were published in Journal of Geophysics Research (Pangia et al., 1990).
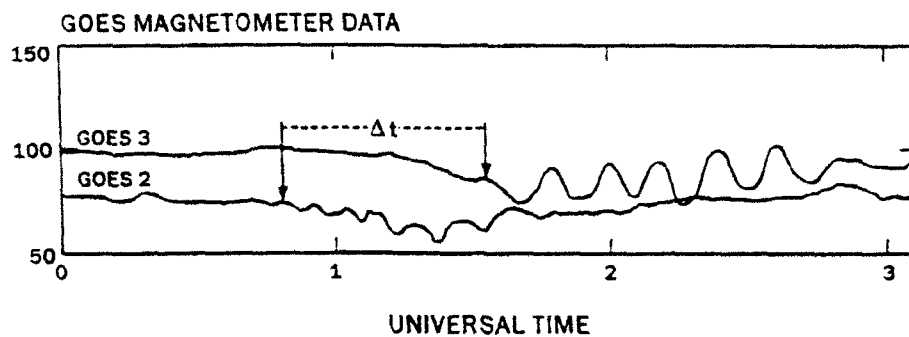
2

SCHEMATIC

SUBSTORM ONSET

GOES-3

GOES-2

|← - - - - - D - - - - - →|← - - - - - - S - - - - - - →|

GOES MAGNETOMETER DATA

GOES 3

GOES 2

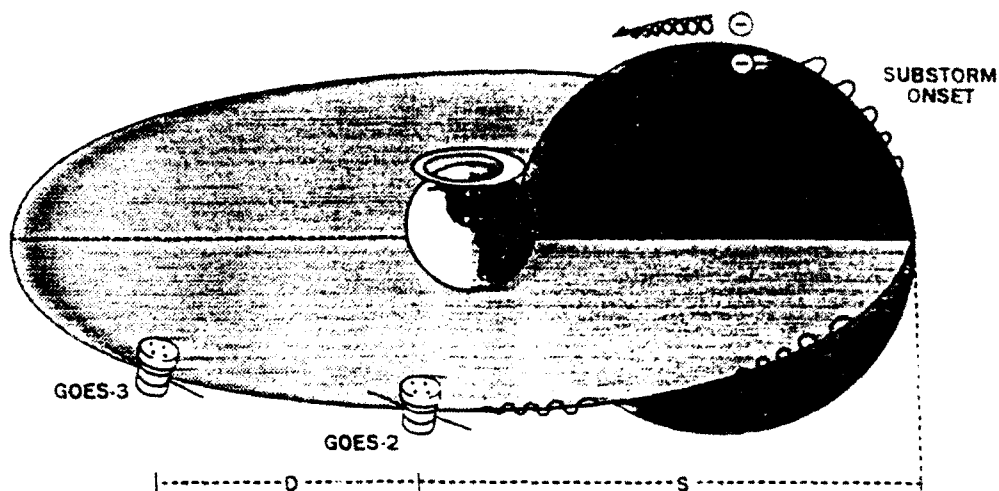Δt

UNIVERSAL TIME

Figure 1: Schematic of determining propagation velocity of low frequency magnetic pulsations by using dual GOES satellites.

3

B Statistical Survey of Propagation Velocity of Storm-time Pc 5 Waves

We conducted a statistical study of propagation velocity of storm time Pc 5 waves observed by dual GOES satellites during the years of 1979, 1983, and 1986. We tabulated the properties of these events and deduced the propagation velocity from the conjunction observations. The GOES satellite data was surveyed to deduce the seasonal variation for the occurrence of Pc 5 wave events and the distribution of propagation velocity over frequency and local time. We also conducted a correlation study to find the relationship between the propagation velocity and wave properties. It is found that the propagation velocity increases with frequency, which increases with the magnetic field inclination angle. The variation of propagation velocity on parameters was also used to determine the wave mode responsible for storm time Pc 5 waves. These results were presented in the 1992 Spring AGU meeting (Lin et al., 1992). These results are described in Section III.

C Theoretical Study of Low Frequency Wave Propagation Velocity

In addition to data analyses, we modeled the wave propagation velocity to better understand the statistical properties of stormtime Pc 5 waves and the correlation between magnetic pulsations and substorm onset. We solved the wave dispersion equation and calculated the wave group velocity for several wave modes that have been suggested to be responsible for exciting stormtime Pc 5 waves. The numerical results are given in Section IV.

D Eigenmode Analysis of Low Frequency Waves in a Dipole Magnetic Field

Since the Earth's dipole magnetic field could limit wave amplitude structure along field lines and thus affect the synchronous satellite observations of magnetic pulsations, we also performed an eigenmode analysis of low frequency waves in a dipole magnetic field. The study shows that stormtime Pc 5 waves have amplitude confined within about $10°$ from the magnetic equator. This result explains that GOES satellites rarely detected stormtime Pc 5 waves during summer months. The calculations are described in Section V.

4

II Remote Diagnostic of Substorm Onsets

Stormtime Pc 5 waves have long been known to be associated with geomagnetic activity (Barfield and Coleman, 1970; Barfield et al., 1972; Barfield and McPherron, 1972). Typically, they occur during the main phase of a geomagnetic storm in the afternoon sector. Barfield and McPherron (1972) compared ATS 1 observations of Pc 5 events to ground magnetograms and found that seventeen of their twenty events studied were closely correlated with the onset of a substorm. The objective of this study is to further investigate this correlation with multiple satellite observations of Pc 5 waves.

Multiple satellite observations offer additional information over single satellite observations regarding propagation characteristics of Pc 5 events (Allan et al., 1982; Walker et al., 1982; Takahashi et al., 1985; Lin and Barfield, 1985). For example, a study of global compressional Pc 5 wave observations by Takahashi et al. (1985) indicates that the waves propagate westward in the afternoon sector with speeds in the range of 4–14 km/s. In a statistical study of stormtime Pc 5 waves, Lin and Barfield (1985) found that the wave propagation speed is typically less than 30 km/s.

For this study, propagation information was used as an additional test of the correlation between stormtime Pc 5 waves and substorm onsets. By using the azimuthal propagation velocity of stormtime Pc 5 waves, we first estimated the substorm onset times and then correlated the estimated onset times with the actual substorm onset times determined from the ground magnetogram data.

A Method

The propagation velocities of stormtime Pc 5 waves in this study were taken from Lin and Barfield (1985), who examined 30 Pc 5 events simultaneously observed by GOES 2 and GOES 3 satellites during the one year interval March 1979 to February 1980. During the study interval, the two satellites were located within approximately 2 hours of local time (approximately $30°$ longitude) of each other. Both satellites were on the geographic equator, with GOES 2 at $104° \pm 4°$ west geographic longitude and GOES 3 at $135°$ west geographic longitude. The onset times of Pc 5 wave events at each satellite T_W were determined to be at the peak of the first magnetic field oscillation. The propagation velocity v_g is then determined from the satellite separation distance D and the time difference between Pc 5 wave event onset times δT_W as

$$v_g = D/\Delta T_W - V,\qquad(1)$$

where $V_s = 3.09$ km/s is the satellite velocity at the synchronous orbit. The error in deducing the wave propagation was found to be mainly due to uncer-

tainties in identifying the first oscillation since the wave amplitude detected by the satellites sometimes grows from a gradual depression of the magnetic field. Therefore, the error of the onset time would be at most one wave period. Using this definition, we found that the error in estimating the propagation velocity is generally less than 15%.

To estimate substorm onset times from Pc 5 propagation speeds, we assume that (1) plasma injection occurs near midnight during substorm onset, (2) the injected plasma excites stormtime Pc 5 waves observed by GOES satellites in the afternoon sector, and (3) the Pc 5 waves propagate at the average drift speed of the injected plasma. These assumptions are based on the satellite observation reported by Lanzerotti et al. (1975) that 1–40 keV protons are associated with a stormtime Pc 5 wave. Furthermore, our study neglects the radial propagation velocity, which may sometimes be appreciable. However, no observation of the radial propagation has been reported.

Since Lin and Barfield (1985) had already surveyed the GOES magnetic field data for stormtime Pc 5 wave events occurring during the one year period, we decided to survey ground magnetometer data during these wave events. Among the 30 wave events in the dataset of Lin and Barfield (1985), we were able to obtain ground magnetometer data near midnight for 18 events. We estimated the time difference between the substorm onset and the GOES observations of the stormtime Pc 5 waves by dividing the distance from GOES 2 to local midnight by the wave group velocity. Extrapolating the wave events to local midnight shows that magnetograms from Russian ground stations were required to conduct this survey. After analyzing these ground magnetograms, we found that magnetic activity was generally present for all the events close to the predicted substorm onset times. However, some ground magnetograms were not suitable for study; we excluded seven events from the study because of highly varying activity, and another five events because of scarce station coverage. We based our study on the six events that showed clear substorm onsets (listed in Table 1).

B   Data Analysis Results

We present two examples of GOES and ground magnetic field data. Figure 2 shows the three components of the GOES magnetometer data for a two hour period starting at 21:30 UT on March 25, 1979 when GOES 2 was at about 14:30 local time. The orientation of the components are that Hp is parallel to the Earth's rotation axis, He is in the radial direction, and Hn completes the orthogonal coordinate system. A Pc 5 wave event with about a seven minute period is seen in the Hp and He components of the GOES 3 measurements from 22:16 to about 22:40 UT. The GOES 2 satellite detected the wave before GOES 3, indicating a westward propagation since GOES 2 was eastward of GOES 3 by 30° in longitude. At GOES 3, the onset time of the wave event was determined to be 22:16 UT at the first peak in the wave train of the

TABLE 1. Comparison of Actual and Estimated Substorm Onset Times

Case	Date	T_W^* (UT)	T_W^* (MLT)	c_g^+ (km/sec)	$T_E^\dagger$ (UT)	$T_S^\ddagger$ (UT)	$T_W - T_S$ (min)	$T_E - T_S$ (min)
1	79-03-25	21:54	14:56	16.3 ± 2.0	$20:11 \pm 15$	19:55	119	16 ± 15
2	79-03-28	22:28	15:28	12.6 ± 1.0	$20:25 \pm 12$	20:45	103	-20 ± 12
3	79-04-21	21:40	14:51	12.1 ± 1.5	$19:18 \pm 21$	19:24	136	-6 ± 21
4	79-11-07	19:41	12:35	9.8 ± 1.3	$16:08 \pm 32$	15:51	196	17 ± 32
5	79-09-26	20:04	13:06	16.8 ± 2.5	$18:01 \pm 19$	17:12	142	19 ± 19
6	79-10-08	23:38	16:32	50.0 ± 10.5	$23:10 \pm 07$	23:24	14	-14 ± 10

$^*T_W$: Pc 5 wave onset time observed by GOES 2 given in both universal time (UT)

and magnetic local time (MLT)

$^\dagger T_E$: Estimated substorm onset time with uncertainty in units of minutes

$^\ddagger T_S$: Actual substorm onset time

^+c_g: Group velocity

All times given to tens of minutes accuracy.

Hp component. The wave onset time at GOES 3 is marked by an arrow in Figure 2. In the GOES 2 data, the first peak of the wave train that can be identified is at 21:54 UT (marked by an arrow in Figure 2). However, the second peak at 21:58 UT is more pronounced and might be considered as the wave onset. In this case, the error in determining the wave onset time at GOES 2 might be four minutes. Using 21:54 UT as the wave onset time at GOES 2, we deduced the wave propagation velocity to be 14 km/s. When we used 21:58 UT as the onset time instead, we obtained 18 km/s for the wave propagation velocity. We therefore chose the average propagation velocity of 16 km/s to estimate the substorm onset time, which was found to be 20:11 UT with an uncertainty of $\pm$ 15 minutes (case 1 in Table 1).

Figure 3 shows ground magnetometer data of the substorm activity that might be associated with the Pc 5 wave event shown in Figure 2 (case 1 in Table 1). We show only the H component of the magnetometer data from five stations during a 14 hour period starting at 17:00 UT, arranged from top to bottom according to geographic longitude ranging from 74° to 41° East. Near local midnight, indicated by an "M," each station showed the negative excursion characteristic of a substorm. The vertical dashed line at 19:55 UT in Figure 3 marks the substorm onset time as determined by the commencement of the negative excursion in the H component near midnight. Note that the estimated substorm onset time (20:11 UT) is 16 minutes later than the actual onset time (within an uncertainty of $\pm$ 15 minutes). Before this onset time, ground magnetometers show no major substorm activity. Therefore, GOES 2

7

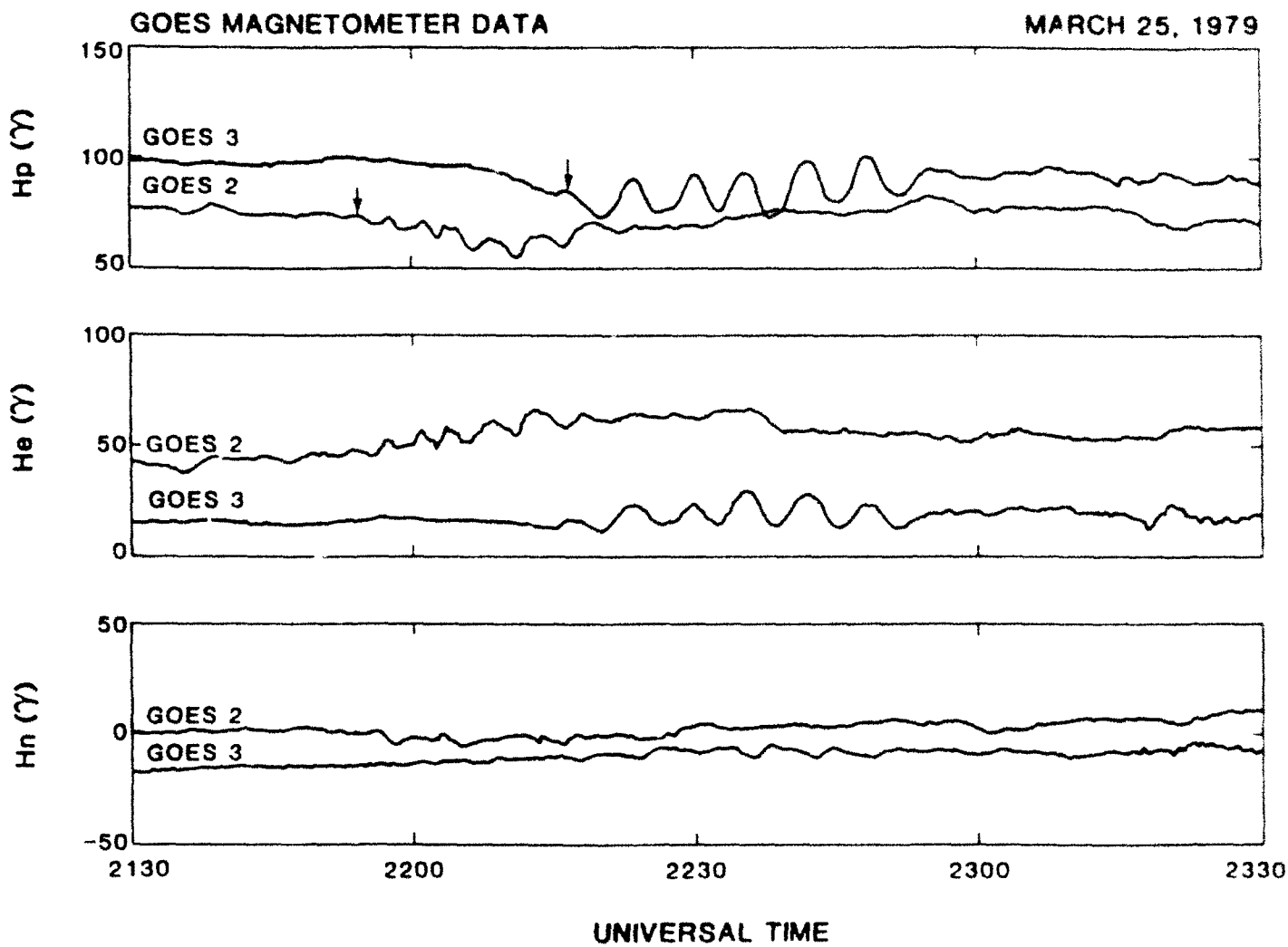**GOES MAGNETOMETER DATA**   MARCH 25, 1979

Figure 2: Magnetic field measurements of a stormtime Pc 5 wave event by dual Goes satellites GOES 2 and 3.

8

observed the Pc 5 event at about 15 hours magnetic local time approximately two hours after the substorm occurred near local midnight.

As the second example (case 6 in Table 1), one hour of GOES magnetometer data starting at 23:30 UT October 8, 1979 are given in Figure 4. This example is difficult to study because ground magnetograms show large substorm activity. The Hp and He components show the first peak of the Pc 5 oscillations starting at 23:47 UT at GOES 3. At the wave onset, GOES 3 was at 14:50 MLT while GOES 2 was at 16:32 MLT. According to the He component, GOES 2 first observed the first wave peak at 23:38 UT with the next peak observed three minutes later. In the same way as case 1, we deduced that this Pc 5 wave event had an average propagation speed of 50 km/s with an uncertainty of $\pm$ 10 km/s. The propagation speed of this event was much higher than that of case 1. From the satellite location and the group velocity, we estimated the substorm onset time to be 23:10 UT with an uncertainty of $\pm$ 7 minutes. Figure 5 displays the ground data for four stations in the same format as Figure 3. The first substorm onset appeared to occur at 20:40 UT, when the first negative excursion bay was detected simultaneously at three stations. Another substorm onset was recorded by Dombas station at 23:24 UT, which is 14 minutes after the estimated substorm onset time. Therefore, the Pc 5 wave event observed by the GOES satellites appears to be correlated with the second substorm onset. We believe that this event is not correlated with the first substorm onset because the GOES satellites had earlier detected another Pc 5 event during 22 UT, much closer to the first substorm onset.

Table 1 summarizes the results obtained by analyzing the six cases for which substorm onset times were reliably identified. Comparison of the wave onset time (given for GOES 2 in Table 1) with the actual substorm time shows that the wave events occurred generally 2–4 hours after the substorm onsets. However, one event (case 6) with a high propagation velocity (50 km/s) occurred only 14 minutes after a substorm onset. Table 1 indicates that a substorm onset occurred within 20 minutes of the estimated substorm onset times. These agreements indicate that the Pc 5 waves and substorm onsets may be correlated.

GROUND MAGNETOMETERS

(N. LAT., E. LONG.)

H COMPONENT

MARCH 25-26, 1979

CAPE KAMENNIYI
(69,74)

TAMBEY
(72,72)

KHARASAVEY
(71,67)

AMDERMA
(70,61)

ARKHANGELSK
(64,41)

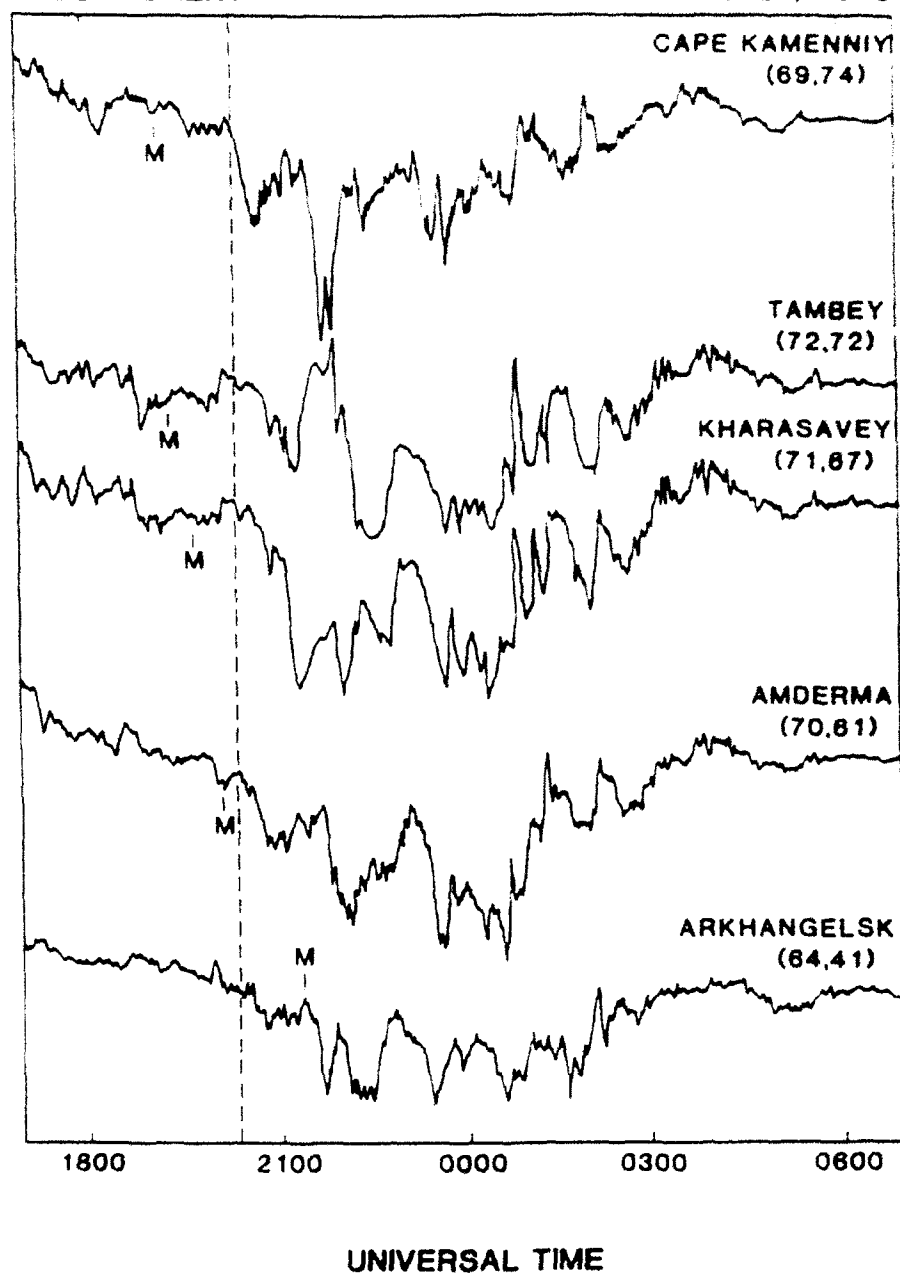1800   2100   0000   0300   0600

UNIVERSAL TIME

Figure 3: Ground magnetometer data in the auroral zone during the stormtime
Pc 5 event shown in Figure 2. Above each magnetogram is the name of the
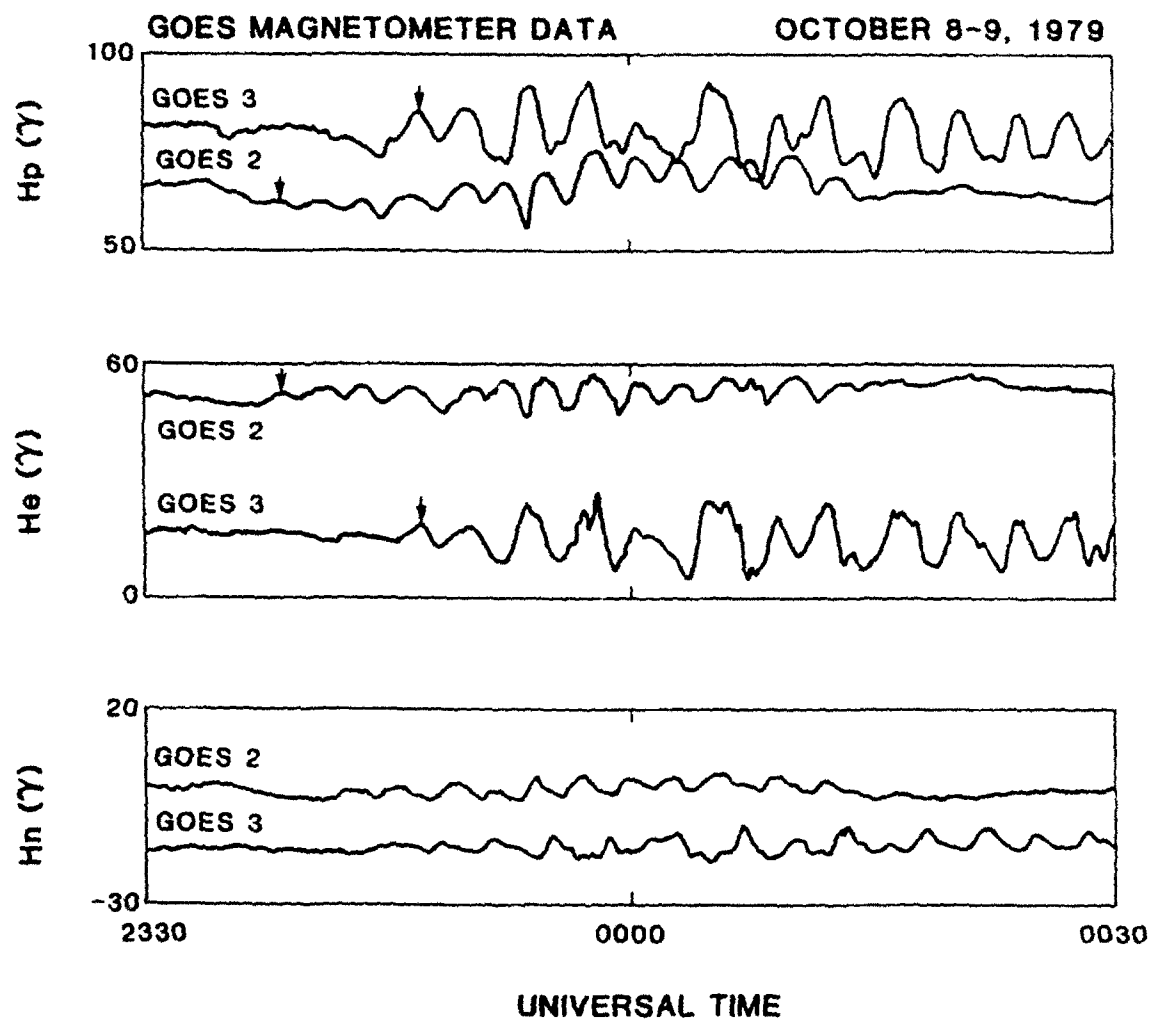station with its geographic latitude and longitude given in parentheses.

Figure 4: Dual Goes satellite observation of a stormtime Pc 5 wave event.

GROUND MAGNETOMETERS   (N. LAT., E. LONG.)

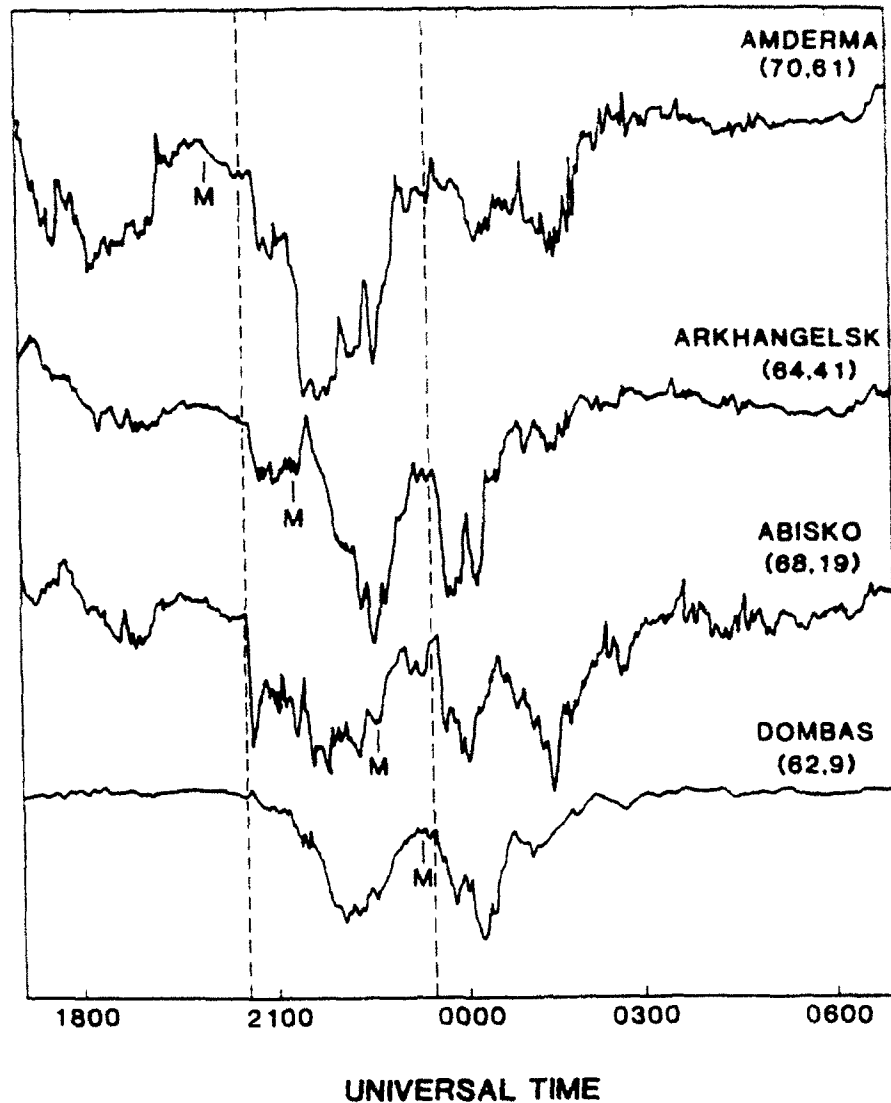H COMPONENT   OCTOBER 8-9, 1979

AMDERMA
(70,61)

ARKHANGELSK
(64,41)

ABISKO
(68,19)

DOMBAS
(62,9)

1800   2100   0000   0300   0600

UNIVERSAL TIME

Figure 5: Ground magnetometer data in the auroral zone during the stormtime
Pc 5 event shown in Figure 4.

12

III Statistical Survey of Propagation Velocity of Stormtime Pc 5 waves

We have analyzed the GOES magnetic field data obtained during the years of 1979, 1983, and 1986. The GOES magnetic field data during these three years are selected because two GOES satellites were separated less than two hours local time. We have scanned the GOES magnetic field data in the year of 1988 for Pc 5 magnetic pulsations but did not include the wave events in the study because two GOES satellites were separated by more than three hours local time. When the satellite separation was more than 3 hours local time, two GOES satellites did not detect Pc 5 wave events simultaneously: often one GOES satellite detected a clear Pc 5 event, while the other GOES satellite merely detected a weak magnetic field depression. This is consistent with the result from the statistical study that stormtime Pc 5 wave events at a single observing point have a duration of less than 2 hours.

We scanned the magnetic field data and found initially 93 events simultaneously detected by two GOES satellites. This initial data set was further narrowed down to 82 events by eliminating events unsuitable for statistical studies. We eliminated events with small wave amplitudes, unclear onsets, or wave frequency higher than 7 mHz. Note that the wave period of Pc 5 pulsations is generally defined in the range of 2 to 10 minutes. After eliminating these events, the data set was reduced to 71 events. These events were then used to deduce the statistical properties. Appendix includes the lists of stormtime Pc 5 events selected for the study.

A Survey Results

The histogram in Figure 6 shows that the propagation velocity of stormtime Pc 5 waves is generally less than 45 km/s. The histogram of propagation velocity distribution has a peak at about 15 km/s. The wave period of stormtime Pc 5 wave events distributes evenly between 2 and 5 minutes (Figure 7), corresponding to a wave frequency in the range between 0.001 and 0.007 Hz. The wave event tends to occur with an average ambient magnetic field between 60 and 120 γ (Figure 8) and an inclination angle between 15 and 60 degrees (Figure 9). Although stormtime Pc 5 events can be detected from noon to midnight, most frequently stormtime Pc 5 waves are detected at local time between 14 and 20 hours (Figure 10).

Figure 11, which is a histogram of wave event duration, indicates that most events have a duration less than 2 hours. For each event, we estimated the propagation velocity v_g and the event duration D. From v_g and D, we then deduced the longitudinal extent of wave region L at synchronous orbit according to the formula $L = v_g D$. Figure 12 shows that a stormtime Pc 5 event typically has a longitudinal extent varying from 30 to 90 degrees.
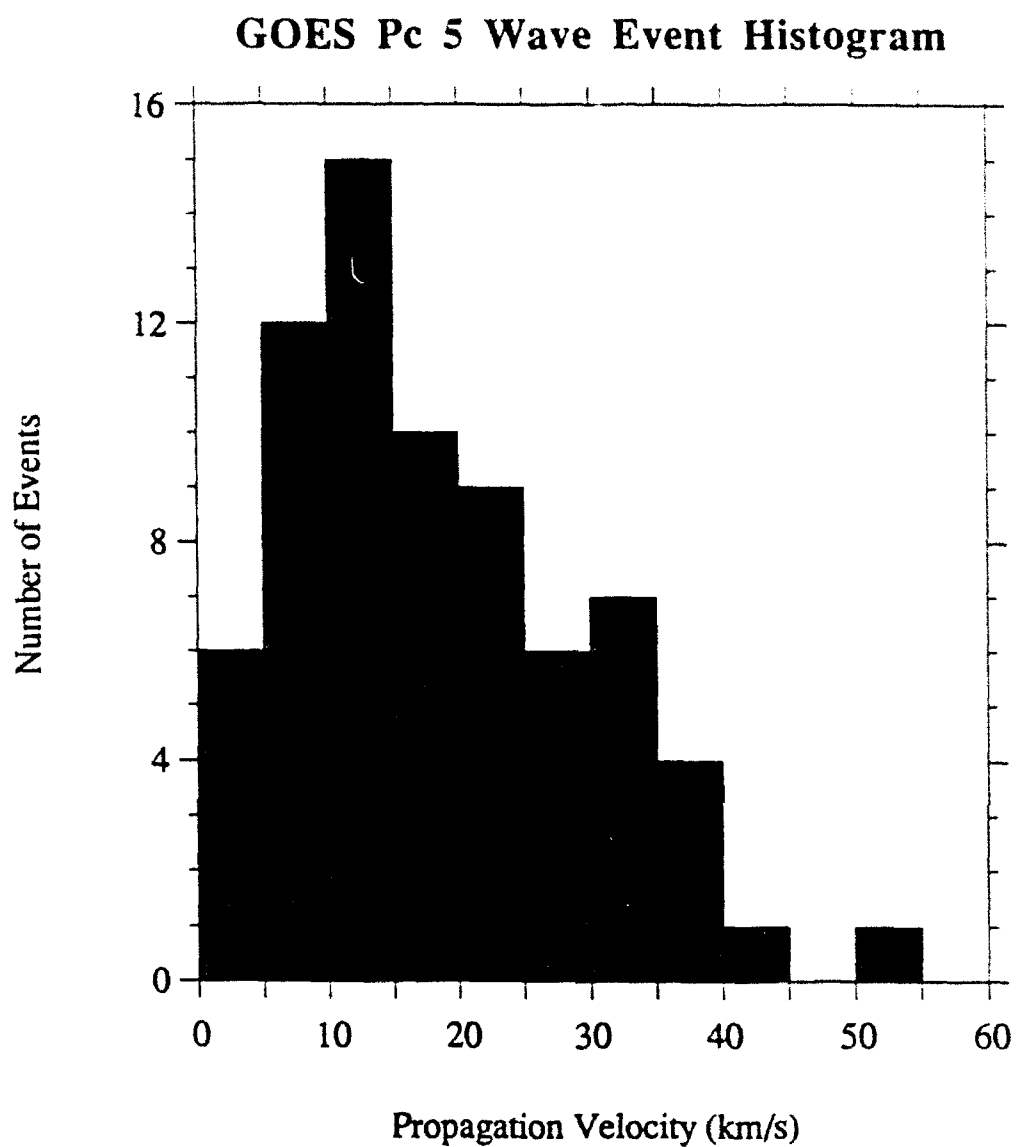
13

GOES Pc 5 Wave Event Histogram

Figure 6: Histogram of propagation velocity of stormtime Pc 5 waves.

GOES Pc 5 Wave Event Histogram
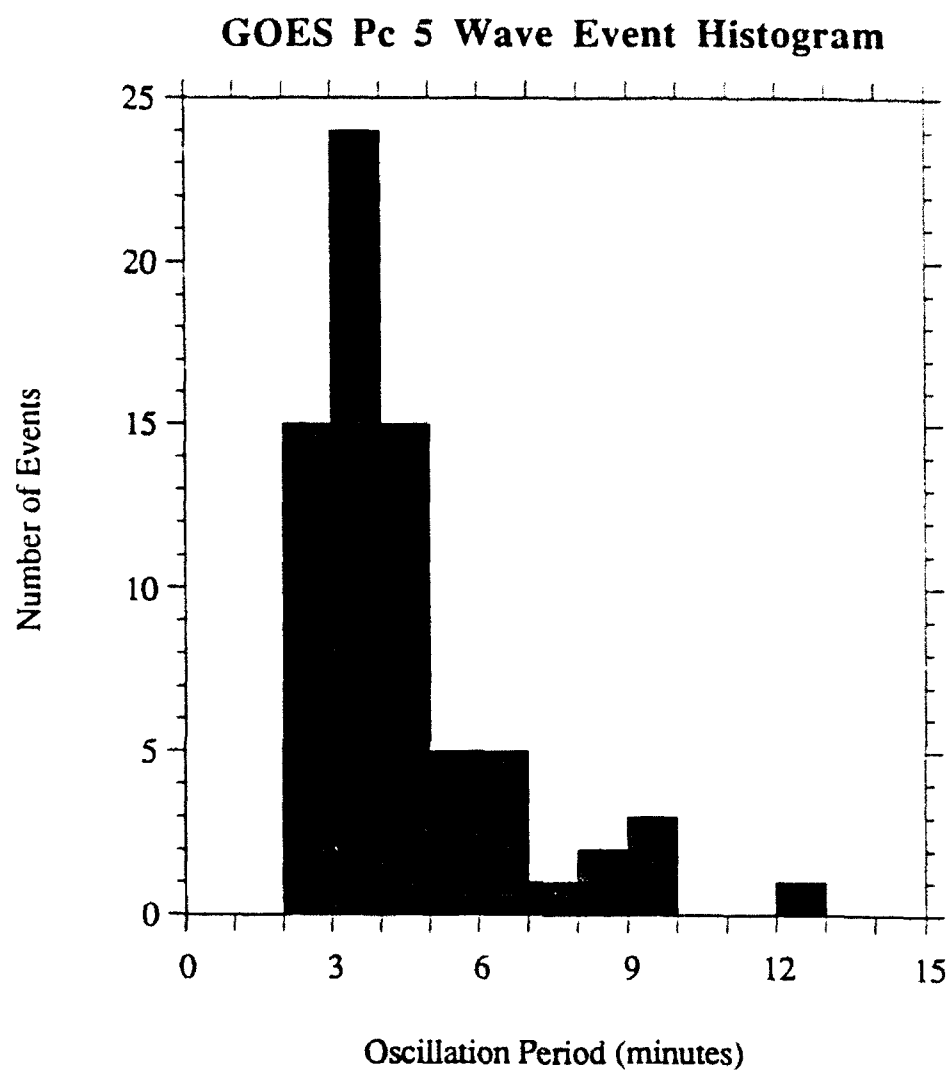
Figure 7: Histogram of wave period of stormtime Pc 5 waves.

GOES Pc 5 Wave Event Histogram
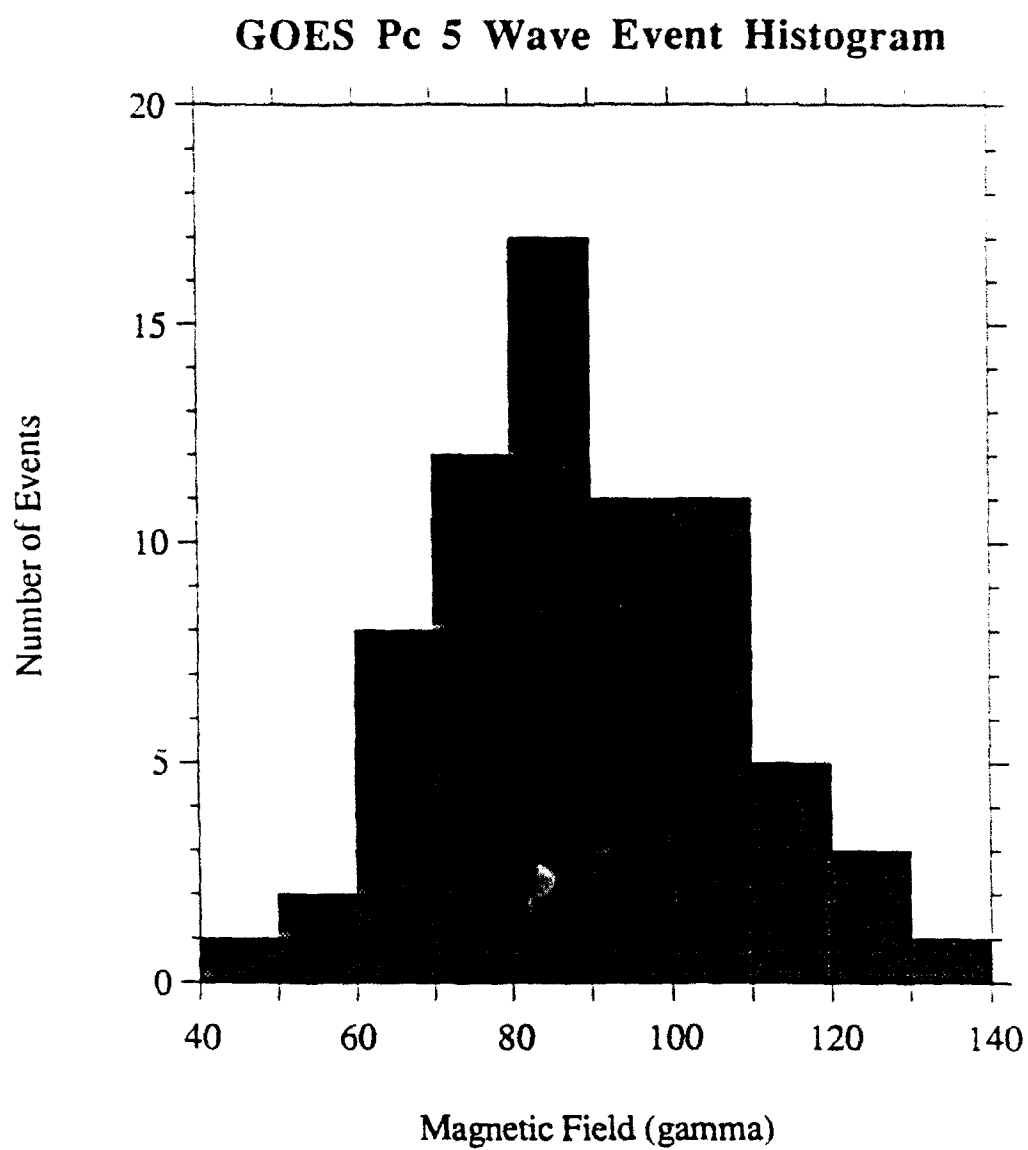
Figure 8: Histogram of average magnetic field during stormtime Pc 5 events.
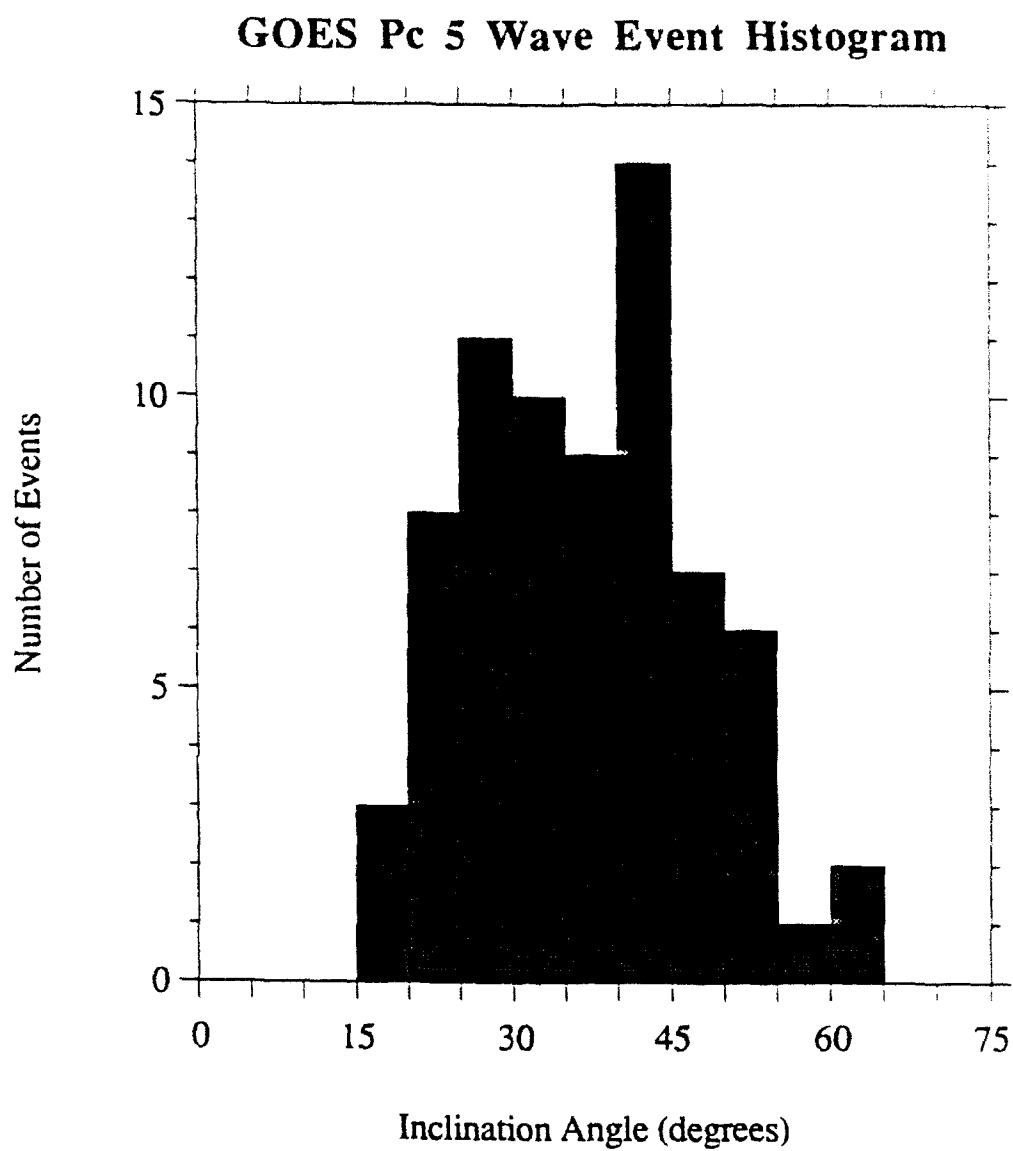
GOES Pc 5 Wave Event Histogram

Figure 9: Histogram of average magnetic field inclination angle during storm-time Pc 5 events.

GOES Pc 5 Wave Event Histogram

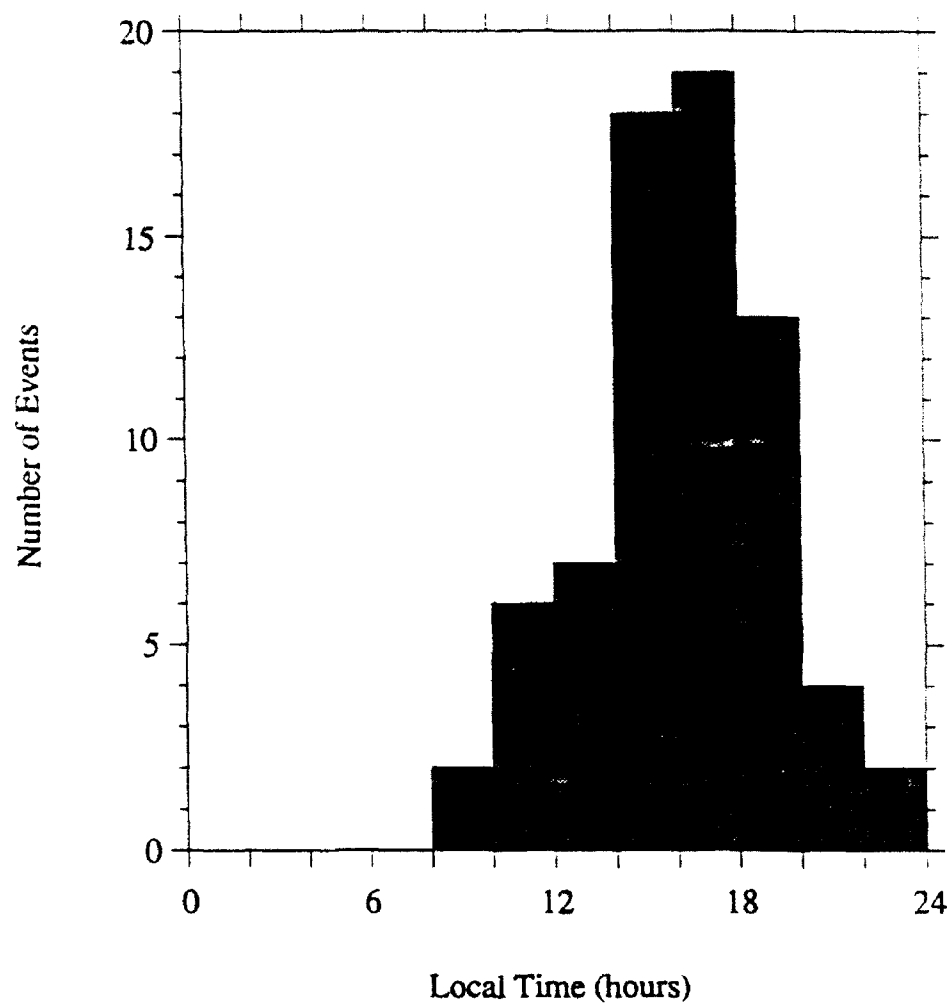Figure 10: Distribution of stormtime Pc 5 events in local time.
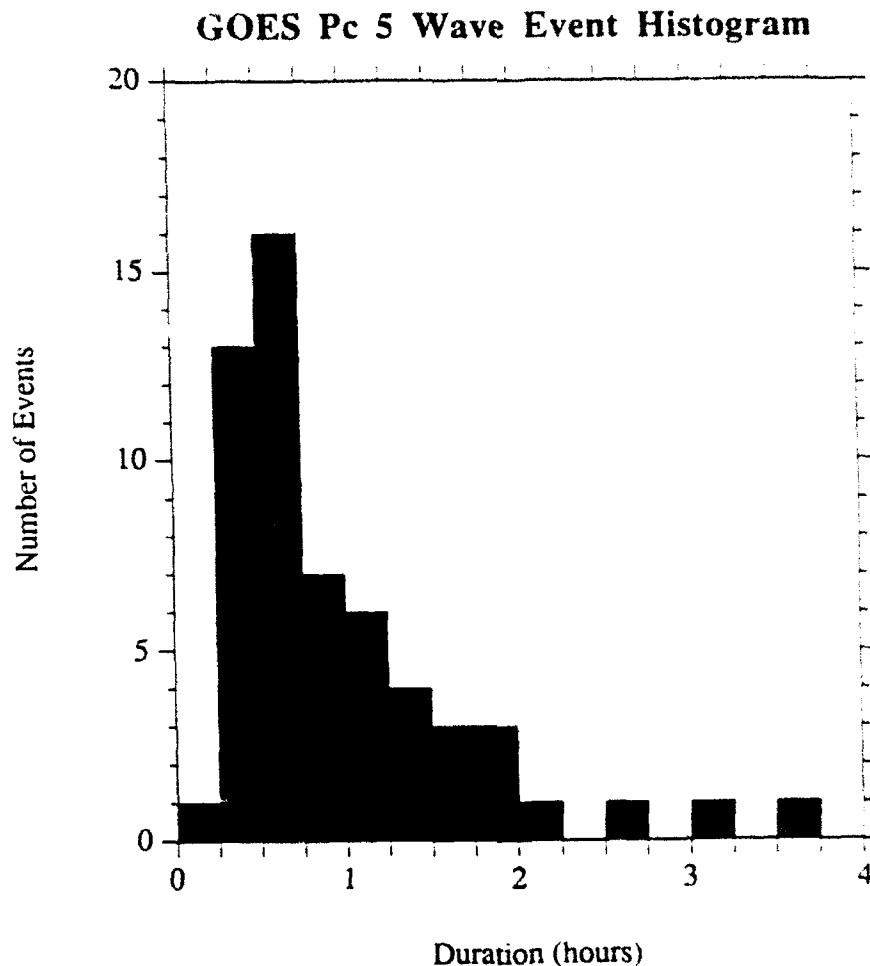
GOES Pc 5 Wave Event Histogram

Figure 11: Histogram of stormtime Pc 5 event duration.

However, a few events have a longitudinal extent as large as 180 degrees.

According to the statistical survey, GOES satellites often observed storm-time Pc 5 events in the winter months from September to April (Figure 13). The data base contains no event in June or July. Since GOES satellites were stationed at the geographic equatorial plane, GOES satellites were at high geomagnetic latitudes during summer months. This figure therefore suggests that stormtime Pc 5 waves are confined at low geomagnetic latitudes. This conclusion is consistent with earlier studies that storm time Pc 5 waves have an eigenmode structure near the equator (Takahashi et al., 1987). Theoretical studies presented in Section V indicate that the wave mode is confined within about 10 degrees around the geomagnetic equator near synchronous orbit.

During stormtime Pc 5 wave events, magnetic field magnitudes are usually comparable at two GOES satellites when they are separated by two hours. However, the inclination angle often varies drastically from the first satellite (closer to midnight) to the second satellite. The histogram given in Figure 14 indicates that the inclination angle at the first satellite distributed evenly between 15 and 55 degress, while the inclination angle at the second satellite was generally between 5 and 25 degrees. This means that the first GOES
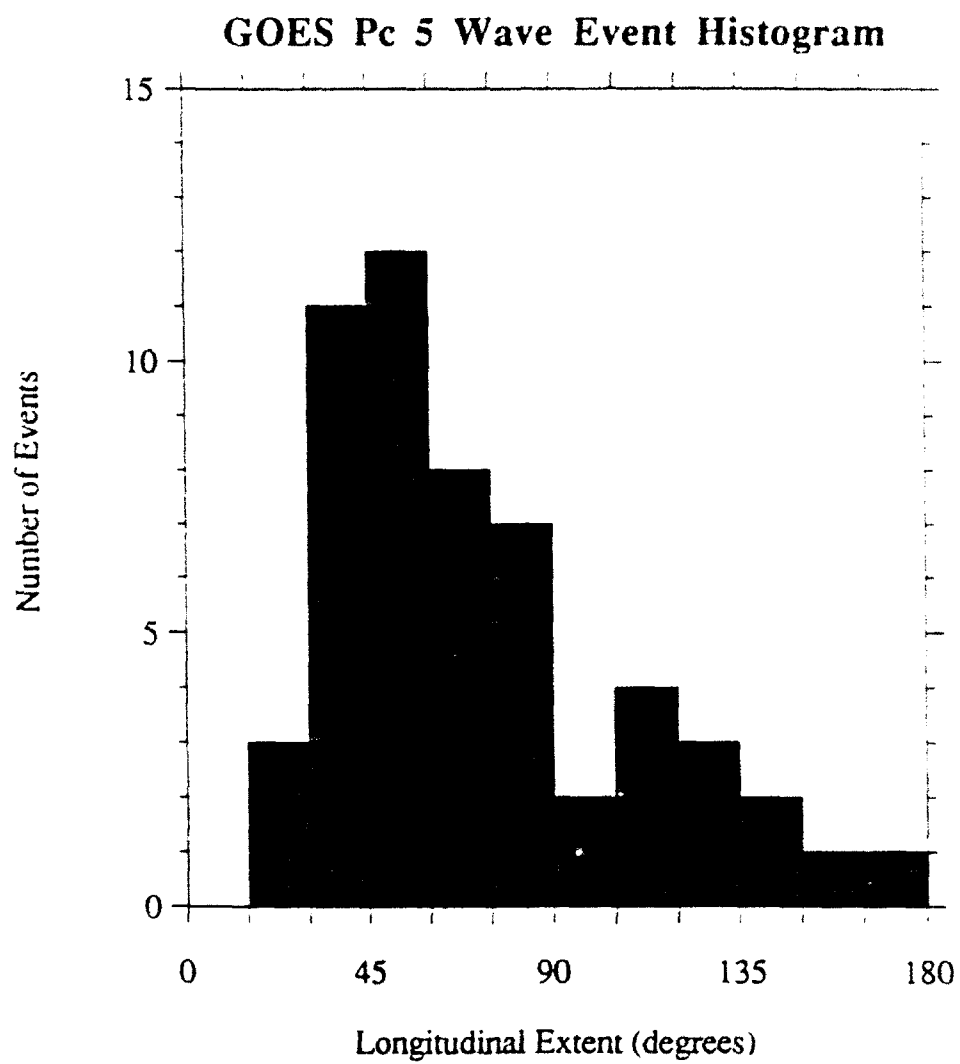
19

GOES Pc 5 Wave Event Histogram

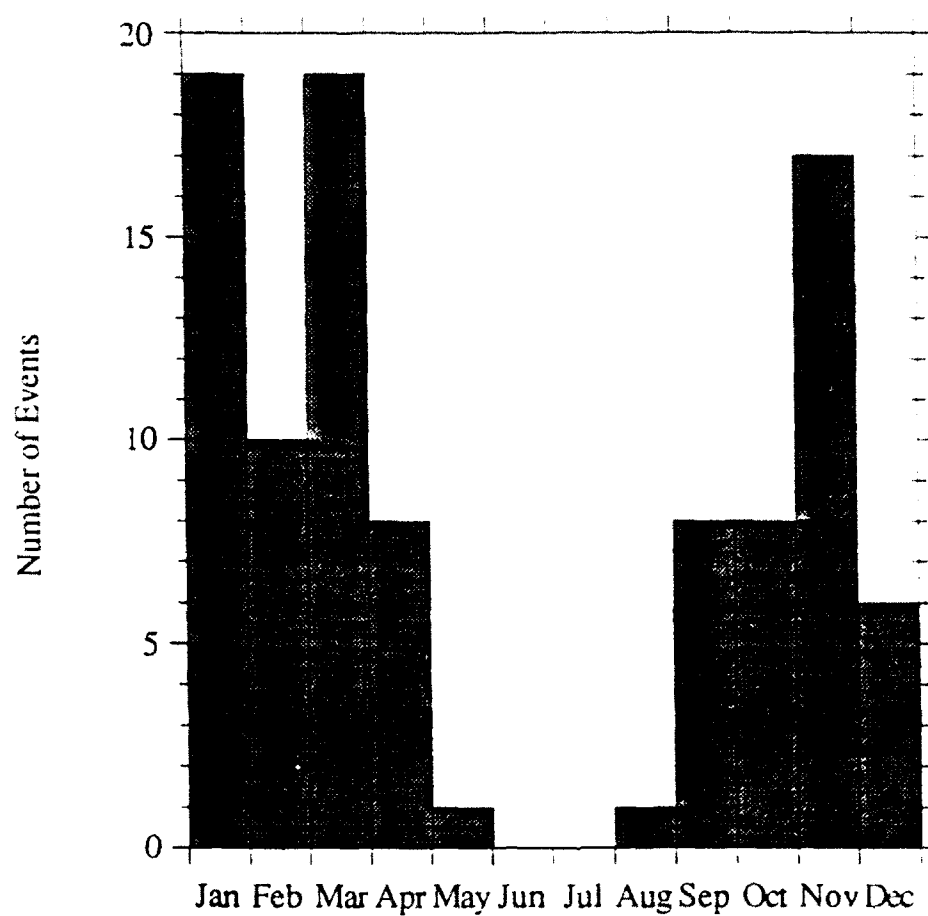Figure 12: Distribution of longitudinal extent for stormtime Pc 5 events.

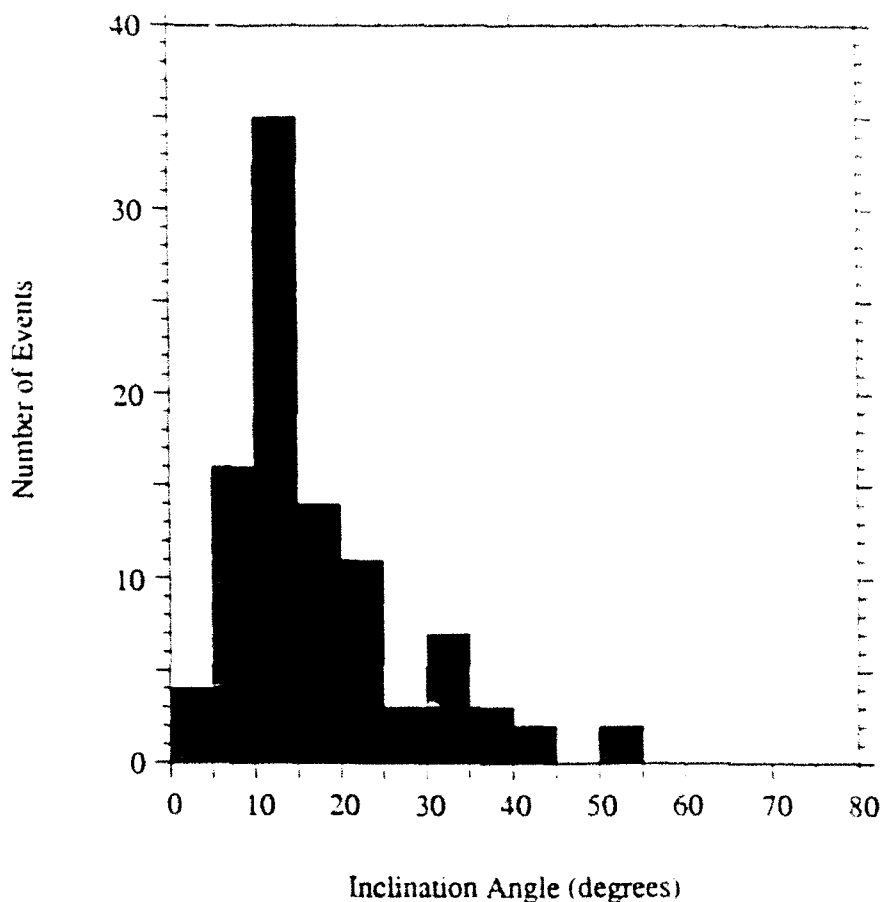Figure 13: Diurnal Distribution of stormtime Pc 5 events.

Figure 14: Distribution of inclination angle observed by GOES satellites during stormtime Pc 5 events. The second GOES satellite was about $30°$ west of the first GOES satellite.

satellite often detected Pc 5 waves with a large tailward magnetic field, while the second GOES satellite would detect the event with a more dipole magnetic field. This result also implies that magnetic field configuration varies sharply from a strong tail field configuration to a relaxed dipole configuration within a two hour local time near dusk.

B Correlation Study

Using the data base and the deduced propagation velocity, we conducted a correlation study of propagation velocity with other observed parameters. The purpose of the correlation study is to find the dependence of propagation velocity on wave and ambient parameters. The variation of propagation velocity on parameters was then used to determine the wave mode responsible for stormtime Pc 5 waves.

Figure 15 plots the propagation velocity in km/s versus wave frequency in Hz. This figure suggests a crude relationship between the propagation velocity
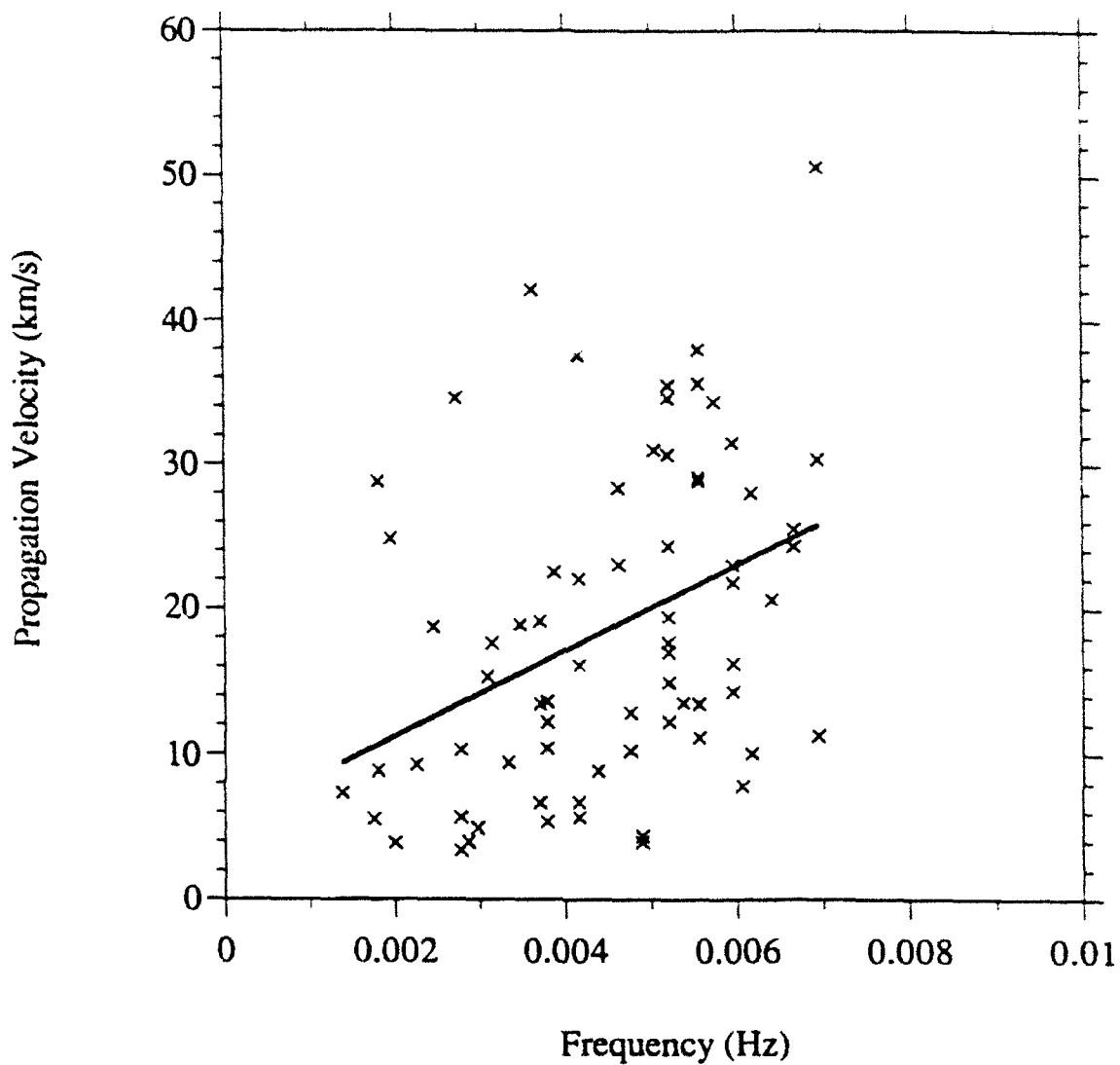
GOES Pc 5 Wave Events

Figure 15: Correlation of propagation velocity and wave frequency for storm-time Pc 5 wave events.

and wave frequency: it shows that the propagation velocity increases linearly with wave frequency. The correlation does not appear to be strong because of a group of outer data points with high propagation velocity. This may mean that more than one class of wave modes are included in the data set.

Furthermore, Figure 15 shows that the wave event scatters over a wide range of propagation velocity for a given wave frequency. The scattering implies that the propagation velocity depends on many parameters. From the dispersion equation, we expect that the propagation velocity depends on frequency, wave number, magnetic field, plasma density and temperature, plasma pressure, plasma beta, magnetic field gradient and curvature, and other parameters.

To further understand the dependence of propagation velocity on other parameters, we correlate propagation velocity with magnetic field in Figure 16, which shows no relationship between propagation velocity and magnetic field magnitude. From this figure, we argue that the propagation velocity would be independent of magnetic field magnitude. We therefore select events in a narrow range of magnetic field between 70 and 90 γ for further studying the correlation between propagation velocity and wave frequency. In this case, we indeed obtained a much better correlation between the propagation velocity and wave frequency, as shown in Figure 17.

Similarly when we used the subset of the data base for $70\gamma < B < 90\gamma$, we found that the propagation velocity increases roughly with the inclination angle. Such a correlation could not be deduced from the complete data set, probably for the same reason that propagation velocity varies with many parameters.

Figure 18 indicates that wave frequency increases with inclination angle I, which is defined as $\tan^{-1}(D/H)$. The D and H components are, respectively, the radial and z component of magnetic field at the geographic equatorial plane. Since D is related to the tail field, the inclination angle increases with tail field. The inclination angle therefore measures the stretch of magnetic field lines due to the enhancement of tail fields during substorms.

We have found that wave frequency of stormtime Pc 5 waves decreases as the events are detected closer toward noon (Figure 19). This correlation is more difficult to interpret because many parameters depend on local time. For example, the inclination angle decreases from midnight toward noon. Since wave frequency is proportional to the inclination angle, wave frequency then decreases toward noon. However, the correlation between wave frequency and local time could be interpreted in several other ways. One plausible explanation is that ring current ions injected during magnetic storms drift toward noon with lower mean energy and a smaller density gradient. As a result, ring current ions excite lower frequency waves toward noon. Since the plasma data is not available for study, we could not make conclusive statements about this possibility.
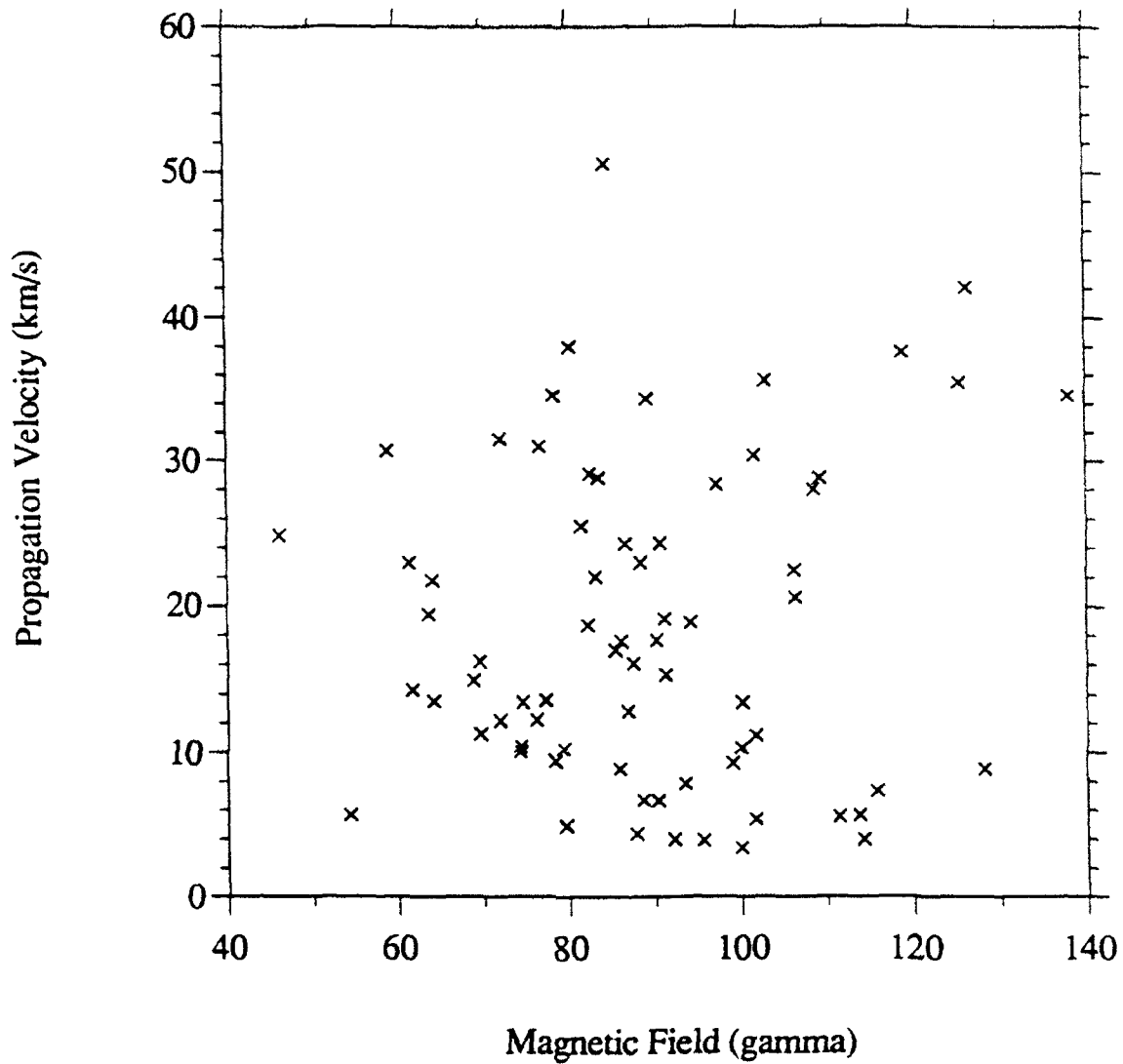
24

GOES Pc 5 Wave Events

Figure 16: Propagation velocity versus magnetic field for stormtime Pc 5 wave events. No correlation is found between propagation velocity and magnetic field for the events studied.

GOES Pc 5 Wave Events

Figure 17: Correlation of propagation velocity and wave frequency for storm-time Pc 5 wave events with magnetic field in the range of 70 to 90 γ.
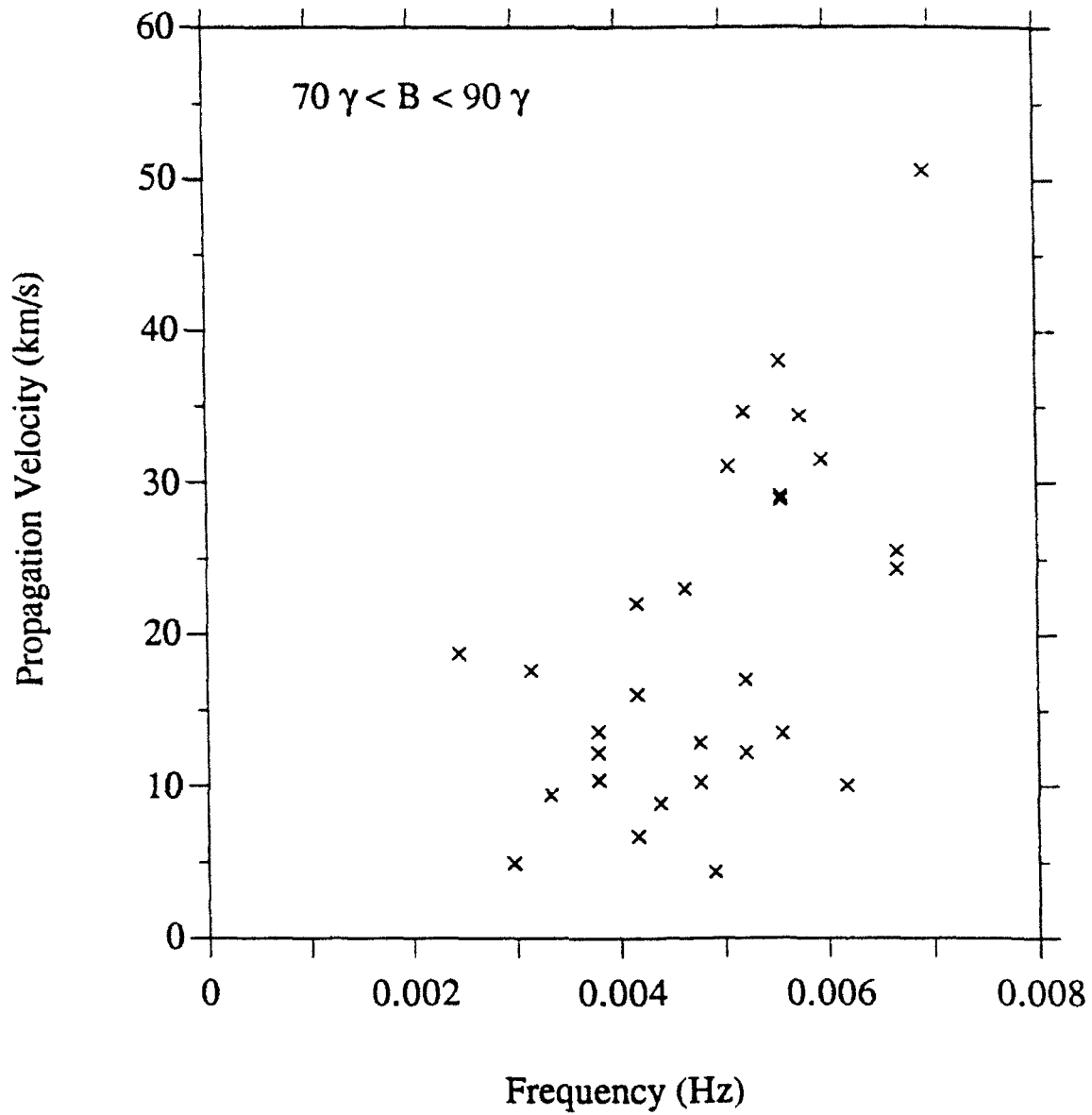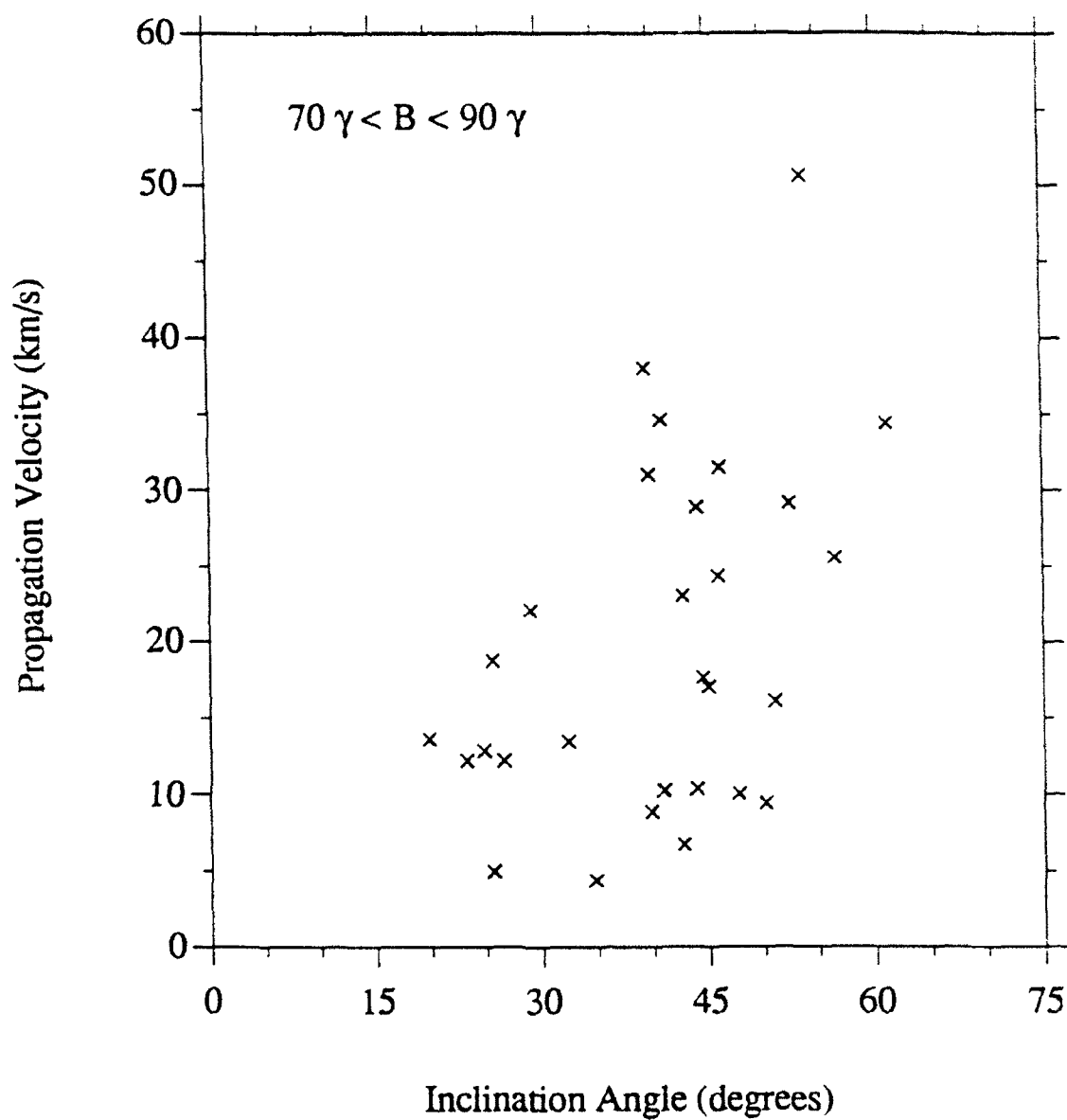
GOES Pc 5 Wave Events

Figure 18: Correlation of propagation velocity and inclination angle for storm-time Pc 5 wave events with magnetic field in the range of 70 to 90 γ.
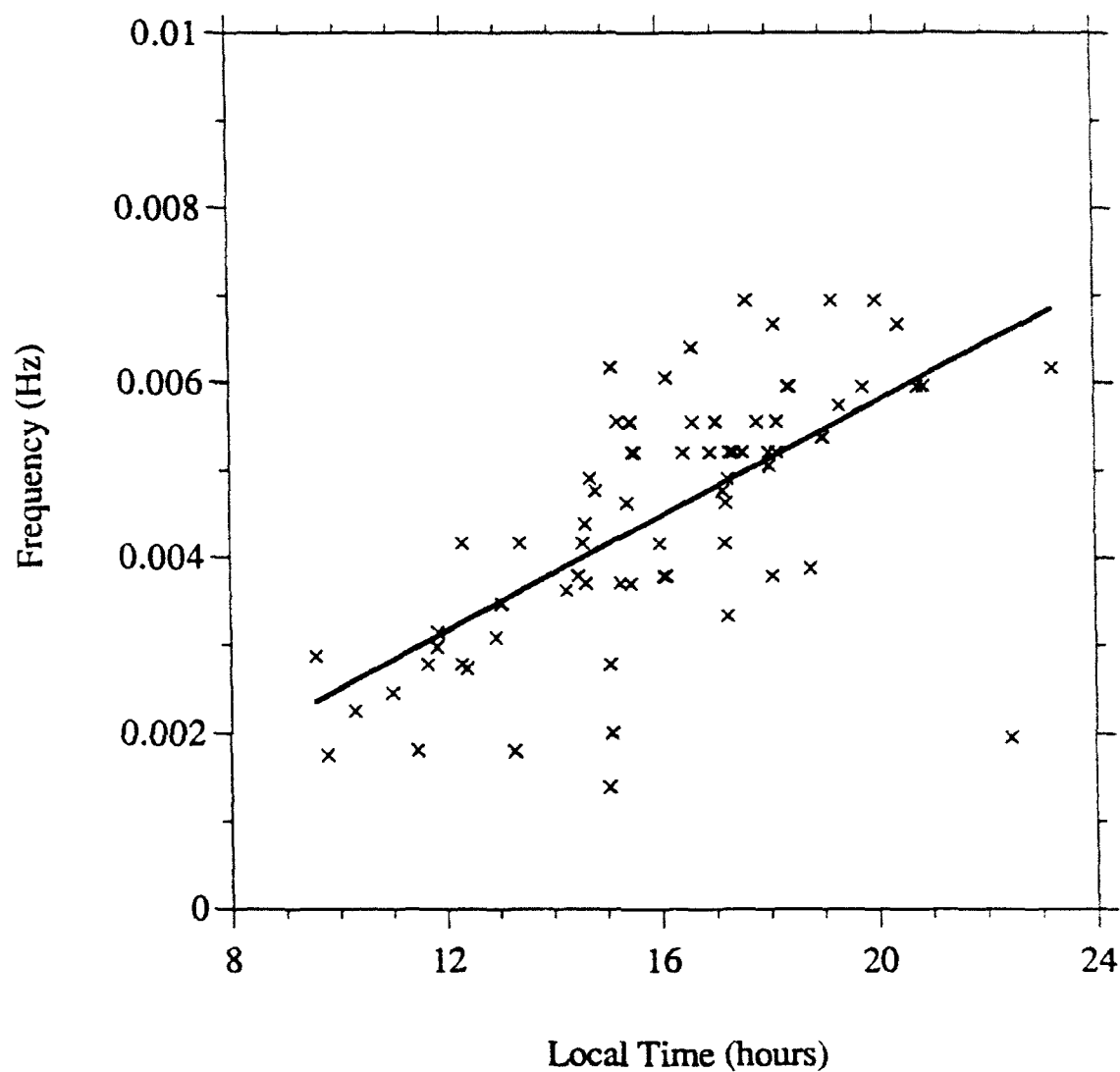
GOES Pc 5 Wave Events

Figure 19: Wave frequency of stormtime Pc 5 wave events versus local time.

IV Theoretical Study of Low Frequency Wave Propagation Velocity

In order to better diagnose substorm onset times, we have modeled the Pc 5 wave propagation velocity in the equatorial region. We first solved the dispersion equation of compressional waves derived from local theory. The numerical results indicate that the propagation speed agrees with the GOES satellite observations. We then compared the wave group velocities for ion drift mode, drift mirror mode, and the low phase velocity drift mode.. In addition, we investigated how the group velocity varies with parallel and perpendicular wave lengths.

A Dispersion Equation

To model wave propagation velocity, we used a general dispersion equation for an inhomogeneous plasma with temperature gradient in a nonuniform magnetic field previously derived by Ng and Patel (1983). This dispersion equation has previously been used to study drift wave instabilities in the magnetosphere.

The plasma is assumed to have a cold plasma density n_c and a hot plasma density n_h, a density gradient scale length r_n, a magnetic field gradient scale length r_b, plasma β, and temperature anisotropy α. We assume the ratio between the density gradient scale length and the perpendicular temperature gradient scale length to be η. The dispersion equation is then

$$D_{11}D_{22} - \frac{\beta_{\perp i}}{2}D_{12}D_{21} = 0 \tag{2}$$

where

$$
\begin{aligned}
D_{11} =\ & \frac{b_i}{\beta_{\|i}}\frac{k_\|^2 V_{\|i}^2}{\omega^2} - b_i\frac{n_c}{n_h} - \sum_j \frac{n_j q_j^2 T_{\perp i}}{n_h q_i^2 T_{\perp j}}\left\{(1-\Gamma_0)\left(1 - \frac{\alpha}{2}\frac{k_\|^2 V_{\|j}^2}{\omega^2}\right)\right. \\
& + \frac{\omega_*}{\omega}(\Gamma_0 - \eta b(\Gamma_0 - \Gamma_1)) - \frac{\omega_d}{\omega}\left[\left(1 - \frac{\omega_*}{\omega}(1-\eta)\right)(\Gamma_0 - b(\Gamma_0 - \Gamma_1))\right. \\
& \left.\left. - \left(\frac{\omega_*}{\omega}\eta + \alpha\frac{\omega_d}{\omega}\right)((2-b)\Gamma_0 - b(3-2b)(\Gamma_0 - \Gamma_1))\right] + \frac{\omega_d^2}{\omega^2}L_{1j}\right\} \\
D_{12} =\ & D_{21} = \sum_j \frac{n_j q_j}{n_h q_i}\left\{\left(1 - \frac{\omega_*}{\omega}(1-\eta)\right)(\Gamma_0 - \Gamma_1) - \left(\frac{\omega_*}{\omega}\eta + \alpha\frac{\omega_d}{\omega}\right)\right. \\
& \left. (\Gamma_0 + (1 - 2b)(\Gamma_0 - \Gamma_1)) - \frac{\omega_d}{\omega}L_{2j}\right\}
\end{aligned}
$$

$$D_{22} = \frac{k^2}{k_\perp^2} - \frac{\omega^2}{k_\perp^2 V_c^2} - \sum_j \beta_{\perp j} \left[\alpha(\Gamma_0 - \Gamma_1) + L_{3j} \right]$$

The parameters are defined as

$$\alpha_j = \frac{T_{\perp j}}{T_{\parallel j}} - 1 \qquad\qquad b_j = \frac{1}{2} k_\perp^2 a_j^2$$

$$a_j = \frac{V_{\perp j}}{\Omega_j} \qquad\qquad v_c^2 = \frac{B^2}{4\pi n_c m_i}$$

$$\beta_{\parallel j} = \frac{8\pi n_j T_{\parallel j}}{B^2} \qquad\qquad \beta_{\perp j} = \frac{8\pi n_j T_{\perp j}}{B^2}$$

$$\Gamma_n = I_n e^{-b} j$$

$$k^2 = k_\parallel^2 + k_\perp^2$$

$$L_j(m, \lambda, \mu) = \frac{1}{2} \int_0^\infty \frac{\omega(1 + \alpha_j) - \omega_{*j}^T - \alpha \omega_{dj} \epsilon}{k_\parallel V_{\parallel j}} Z J_\lambda J_\mu \epsilon^m e^{-\epsilon} \, d\epsilon$$

$$L_{1j} = 2L_j(2, 0, 0)$$

$$L_{2j} = \frac{4}{k_\perp a_j} L_j(3/2, 1, 0)$$

$$L_{3j} = \frac{2}{b_j} L_j(1, 1, 1)$$

$T_\perp$ and $T_\parallel$ are respectively the perpendicular and parallel temperatures, Z is the usual plasma dispersion function with argument $(\omega - \omega_{dj}\epsilon)/(k_\parallel V_{\parallel j})$, J_0 and J_1 are the zeroth and first-order Bessel functions with arguments $k_\perp a_j \epsilon^{1/2}$; I_0 and I_1 are modified Bessel functions with arguments b_j. The drift frequencies

have usual meaning.

$$\omega_{*j} = \frac{k_y V_{\perp j}^2}{2\Omega_j r_n}$$

$$\omega_{dj} = \frac{-k_y V_{\perp j}^2}{2\Omega_j r_B}$$

$$\omega_{*j}^T = \omega_{*j}[1 - \eta_j(1 - \epsilon)]$$

and

$$r_B = 2 \left[\sum_j \beta_{\perp j}(1 + \eta_j) \right]^{-1} r_n$$

$$r_n = \left[\frac{d \ln n}{dx} \right]^{-1}$$

B   Numerical Solutions

For a given parallel wave length, we first solved numerically Equation 2 for wave frequency as a function of perpendicular wave number $k_\perp$. We then calculated the perpendicular group velocity V_g from the relationship

$$V_g = \partial\omega/\partial k_\perp \qquad (3)$$

The propagation velocity is examined for three wave modes: ion drift, drift mirror and the low phase velocity drift modes. The parameters used in the calculation are: density ratios n_{hi}/n_{ci} and $n_{he}/n_{ce} = 0.01$, η_i and $\eta_e = -3.0$, $r_n = 50$ and temperature anisotropy $A = 0$, $\beta_\parallel = 1$, $T_i = 10$ keV, and $b_i = 1/2(k_\perp \rho_i)^2 = 0.1$. The solutions of the dispersion equation for various parameters are shown in Figures 20–26.

B.1   Ion Drift Mode

Figure 20 shows the wave frequency (solid line) and growth rate (dashed line) as a function of perpendicular wave vector times the ion gyroradius $k_\perp \rho_i$ for the ion drift mode. For the ion drift mode, the frequency is positive for positive wave mode number and thus the wave phase velocity is in the direction of the ion diamagnetic drift. For this mode, the parallel wave number is very small and thus the wave mode has a long parallel wave length. This figure indicates that the instability occurs at very small parallel wave number ($k_\parallel \rho_i < 0.006$) and the growth rate decreases with $k_\parallel$. The wave frequency of growing waves ω normalized by $k_\parallel v_i$ decreases from 3 to 1 as $k_\parallel \rho_i$ increases from 0.002 to 0.006.
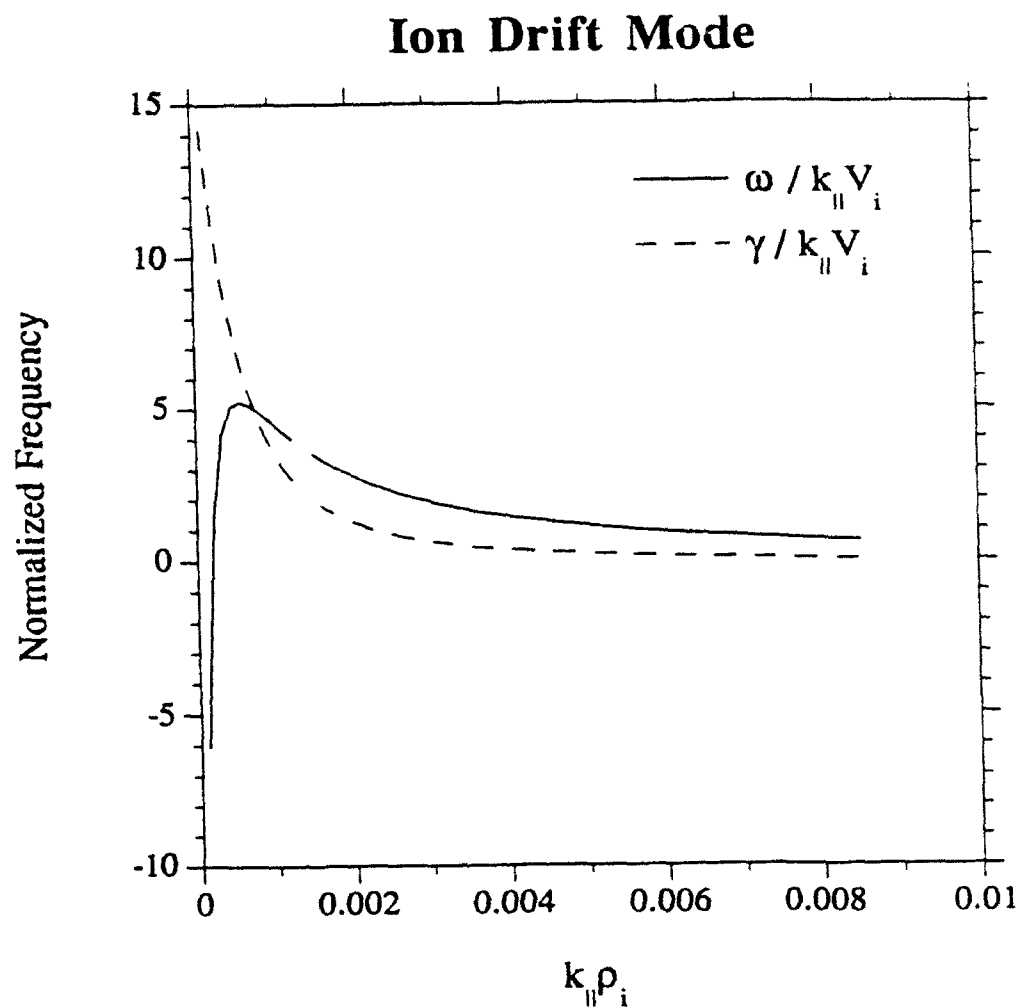
31

Ion Drift Mode

Figure 20: Wave frequency and growth rate as a function of the parallel wave vector for the ion drift mode.
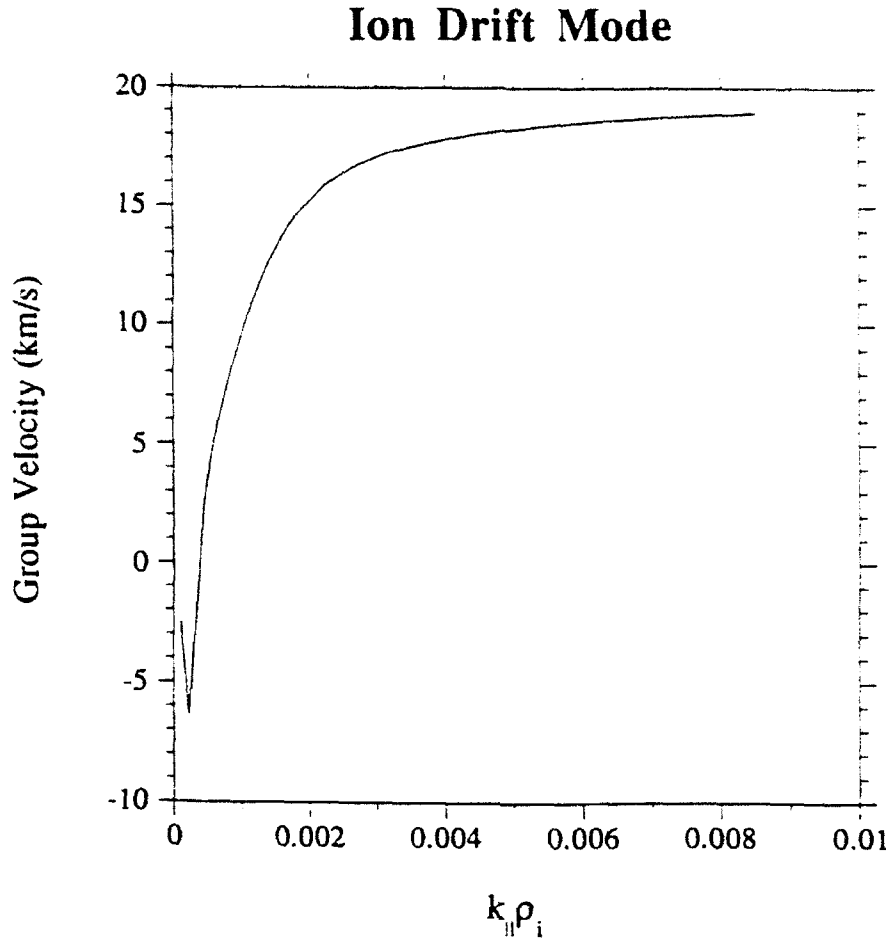
Ion Drift Mode

Figure 21: Perpendicular group velocity as a function of the parallel wave vector for the ion drift mode.

However, according to the GOES observations, the wave is confined to $10°$ latitude. The parallel wave number $k_{\parallel}\rho_i$ should be greater than 0.04 for a typical ion temperature of 10 keV. Therefore, ion drift waves have difficulties in explaining the parallel wavelengths of the Pc 5 waves observed by GOES satellites.

For the ion drift mode, the group velocity increases with the parallel wave number $k_{\parallel}$ (Fig 21). For $k_{\parallel}\rho_i = 0.002$, when the ion drift mode has a large growth rate, the perpendicular group velocity is less than 10 km/s. Since most propagation velocity for stormtime Pc 5 waves are greater than 10 km/s, the GOES satellite observations suggest that ion drift mode could not account for stormtime Pc 5 waves with large propagation velocity.

In Figure 22, we plot the frequency and growth rate as a function of $k_{\perp}\rho_i$ for the ion drift mode. The parameters are the same as Figure 20 except that $k_{\parallel}\rho_i = 0.002$ is chosen. This figure indicates that the ion drift waves are unstable for $k_{\perp}\rho_i < 1$. In Figure 23, we next present the perpendicular group velocity as a function of $k_{\perp}\rho_i$ for the ion drift mode. The perpendicular group velocity increases from 10 km/s to about 20 km/s as $k_{\perp}\rho_i$ increases from 0.1
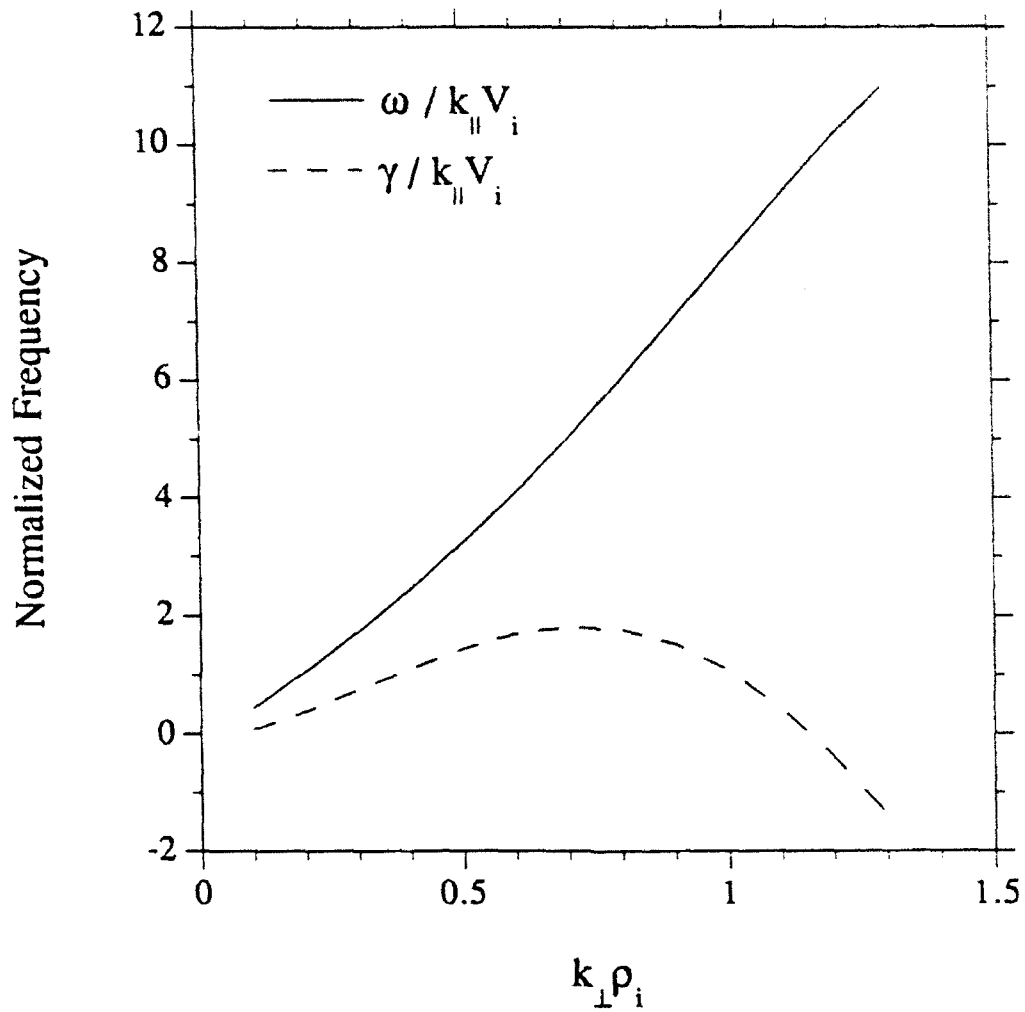
33

Ion Drift Mode

Figure 22: Wave frequency and growth rate as a function of the perpendicular wave vector for the ion drift mode.
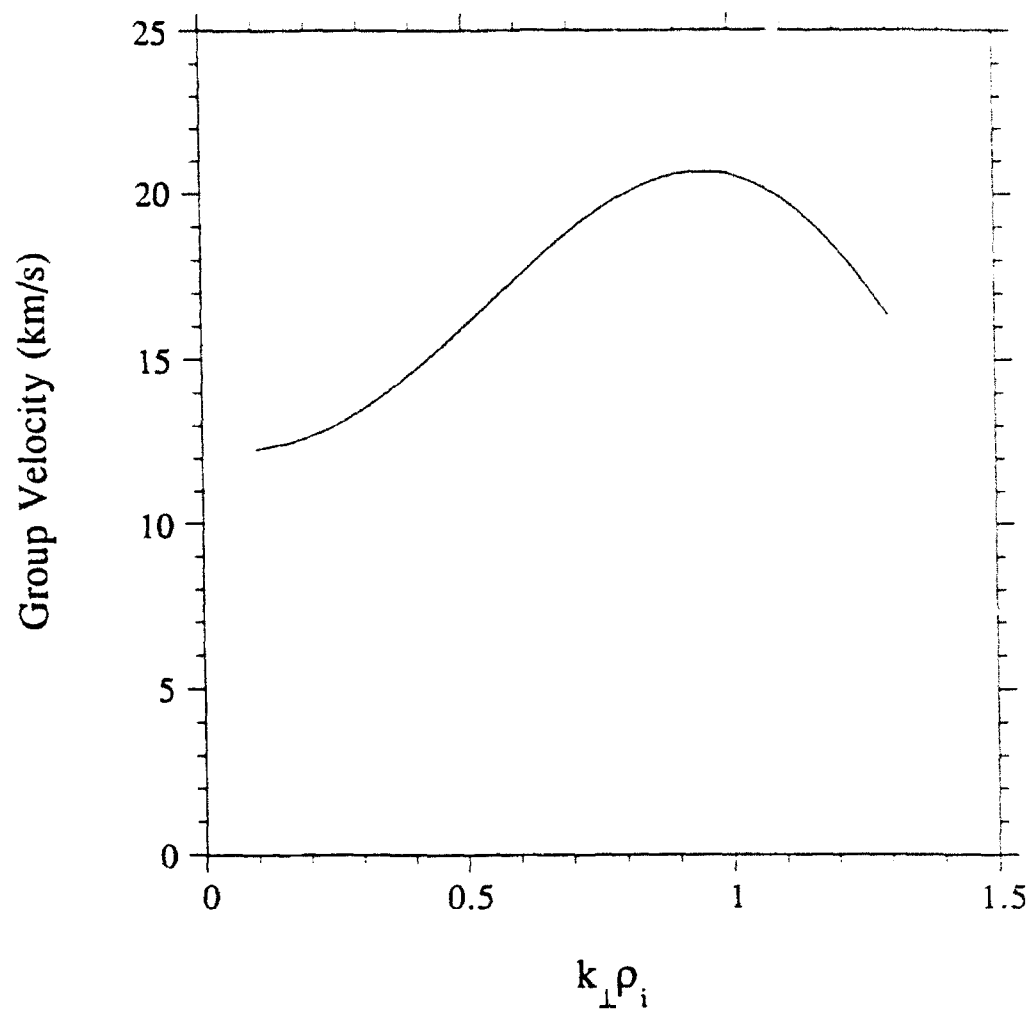
Ion Drift Mode

Figure 23: Perpendicular group velocity as a function of the perpendicular wave vector for the ion drift mode.

Drift Mirror Mode

Figure 24: Wave frequency and growth rate as a function of the parallel wave vector for the drift mirror mode.

to 1. Since Pc 5 waves generally have a wave propagation velocity less than 50 km/s. it is likely that the perpendicular wavelength needs to be greater than the ion gyroradius such that $k_\perp \rho_i < 1$. It is generally expected that $k\rho_i$ is less than 1. The statistical survey suggests that the perpepndicular propagation velocity varies from 5 km/s to 40 km/s and for about half of the event- the propagation velocity is less than 20 km/s.

B.2 Drift Mirror Mode

We next investigate propagation velocity for the drift mirror mode. Figure 24 plots the frequency and growth rate as a function of $k_{\parallel}\rho_i$ for the drift mirror mode. For the drift mirror mode. which is unstable for a plasma with a temperature anisotropy. we chose the following parameters: density ratios n_{hi}/n_{ci} and $n_{he}/n_{ce} = 0.01$. density gradient scale length $r_n = 50$. temperature anisotropy $A = 1.5$, $\beta_{\parallel} = 1$. $T_i = 10$ keV. and $b_i = 1/2(k_\perp \rho_i)^2 = 0.1$. To separate the effects of drift mirror mode from those of ion drift mode. we examie the case in the absence of temperature gradients (η_i and $\eta_e = 0$).

36

Drift Mirror Mode

Figure 25: Perpendicular group velocity as a function of the parallel wave vec⁺or for the drift mirror mode.

For a given $k_\perp \rho_i$, the drift mirror waves are unstable for all $k_\parallel \rho_i$, and the wave frequency is much less than $k_\parallel v_i$ ($\omega/k_\parallel v_i \ll 1$) (Figure 21). The growth rate $\gamma/k_\parallel v_i$ also decreases with increasing $k_\parallel \rho_i$. For the same parameters, the perpendicular group velocity as a function of $k_\parallel \rho_i$ for the drift mirror mode is shown in Figure 25. As $k_\parallel \rho_i$ increases from 0.05 to 0.3, the perpendicular group velocity decreases from 60 km/s to about 10 km/s. In the range of $k_\parallel \rho_i < 0.5$, the perpendicur group vlocity is between 5 to 60 km/s. The calculted range of p∋rpendicular group velocity therefore agrees with the observations.

We next examine the dependence of drift mirror mode on wave perpendicular wavelength. Figure 26 plots the frequency and growth rate as a function of $k_\perp \rho_i$ for the drift mirror mode. In this figure, we used $k_\parallel \rho_i = 0.2$ and other parameters the same as Figure 24. Figure 27 plots the perpendicular group velocity as a function of $k_\perp \rho_i$ for the drift mirror mode. The perpendicular group velocity increases from 5 km/s to about 30 km/s as $k_\perp \rho_i$ increases from 0.1 to 0.6. In the range of $k_\perp \rho_i < 1$, the perpendicur group vlocity $V_{g\perp}$ is between 5 to 30 km/s. The perpendicular group velocity i₃ maximum when $k_\perp \rho_i = 0.6$. For $k_\perp \rho_i > 0.6$, perpendicular group velocity $V_{g\perp}$ decreases with

Drift Mirror Mode

Figure 26: Wave frequency and growth rate as a function of the perpendicular wave vector for the drift mirror mode.

Drift Mirror Mode
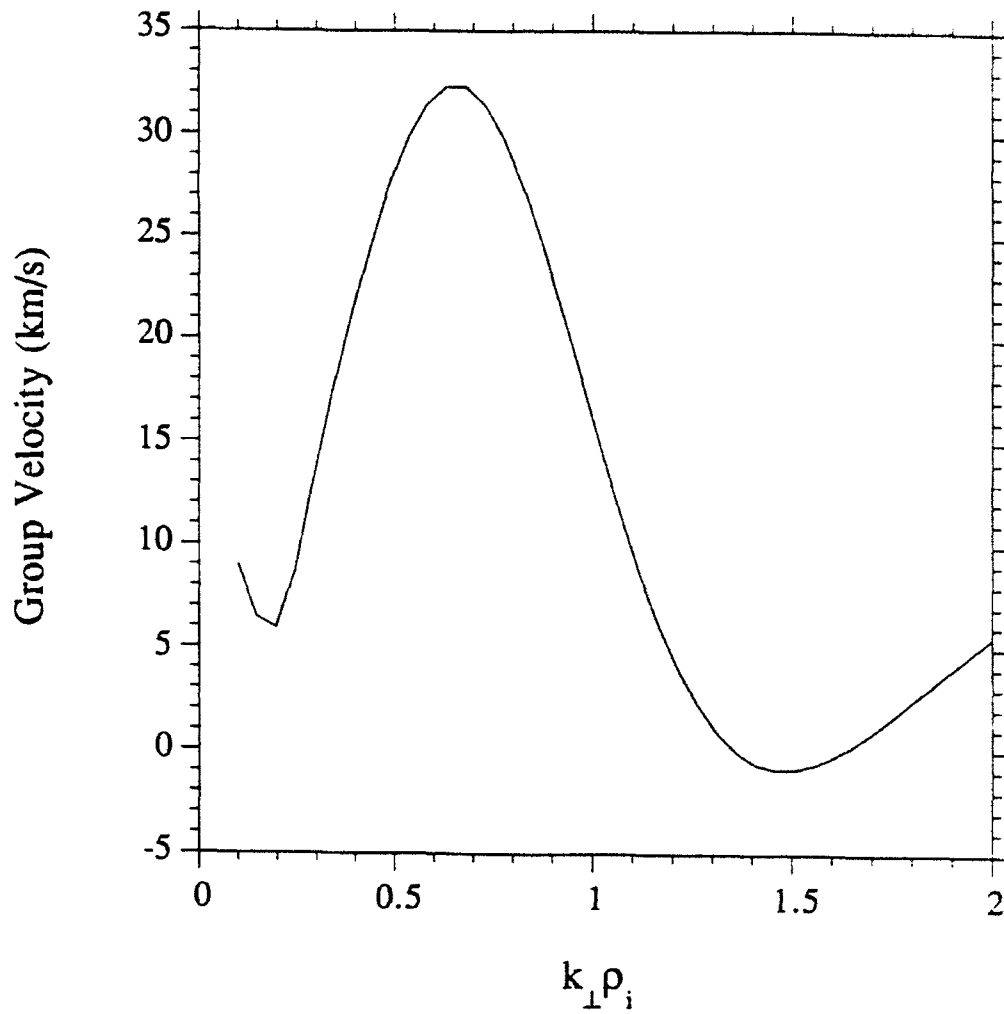
Figure 27: Perpendicular group velocity as a function of the perpendicular wave vector for the drift mirror mode.
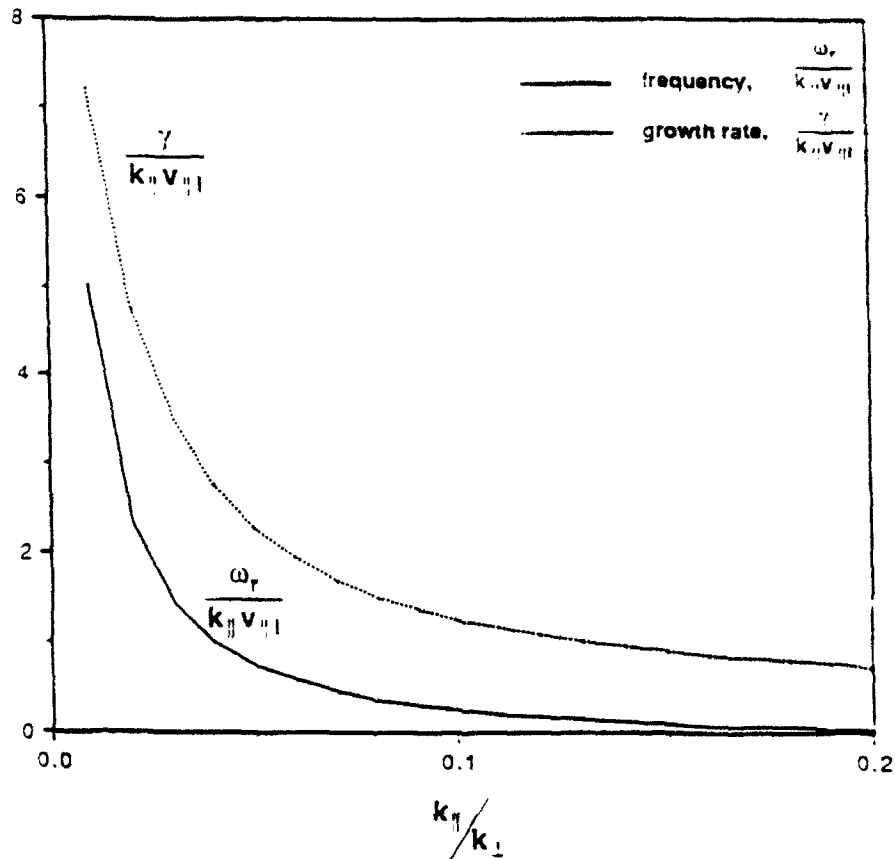
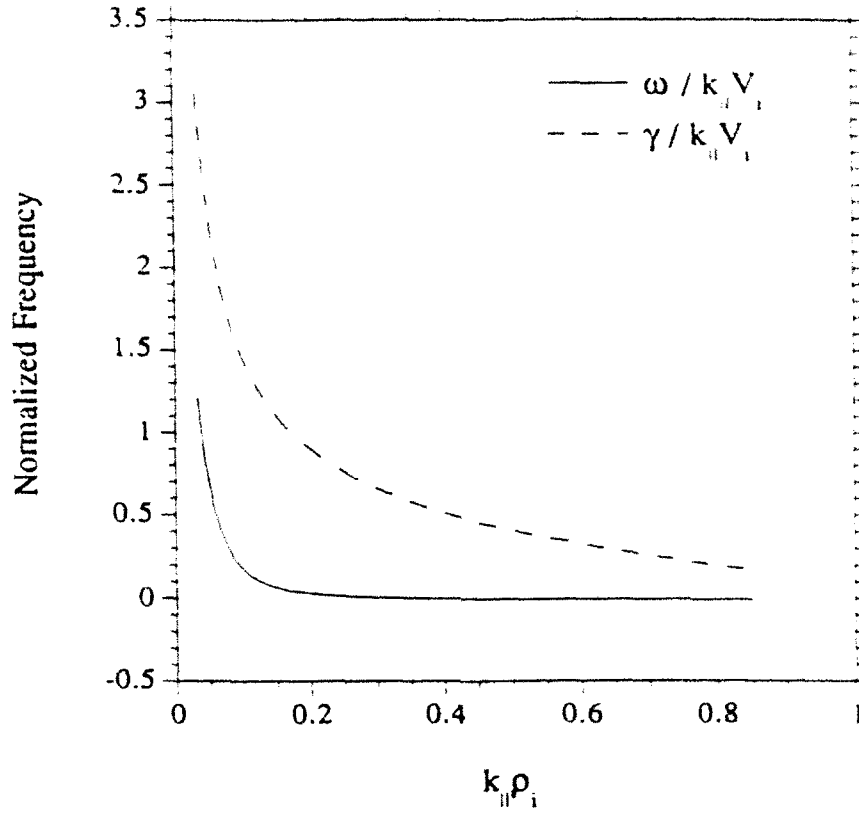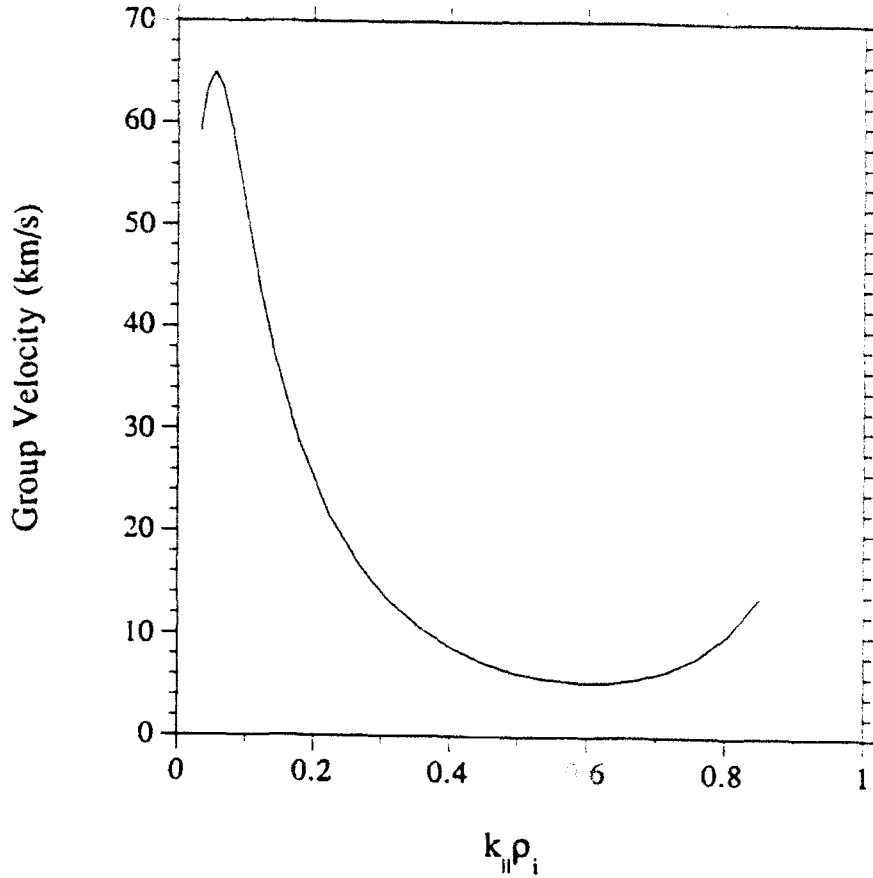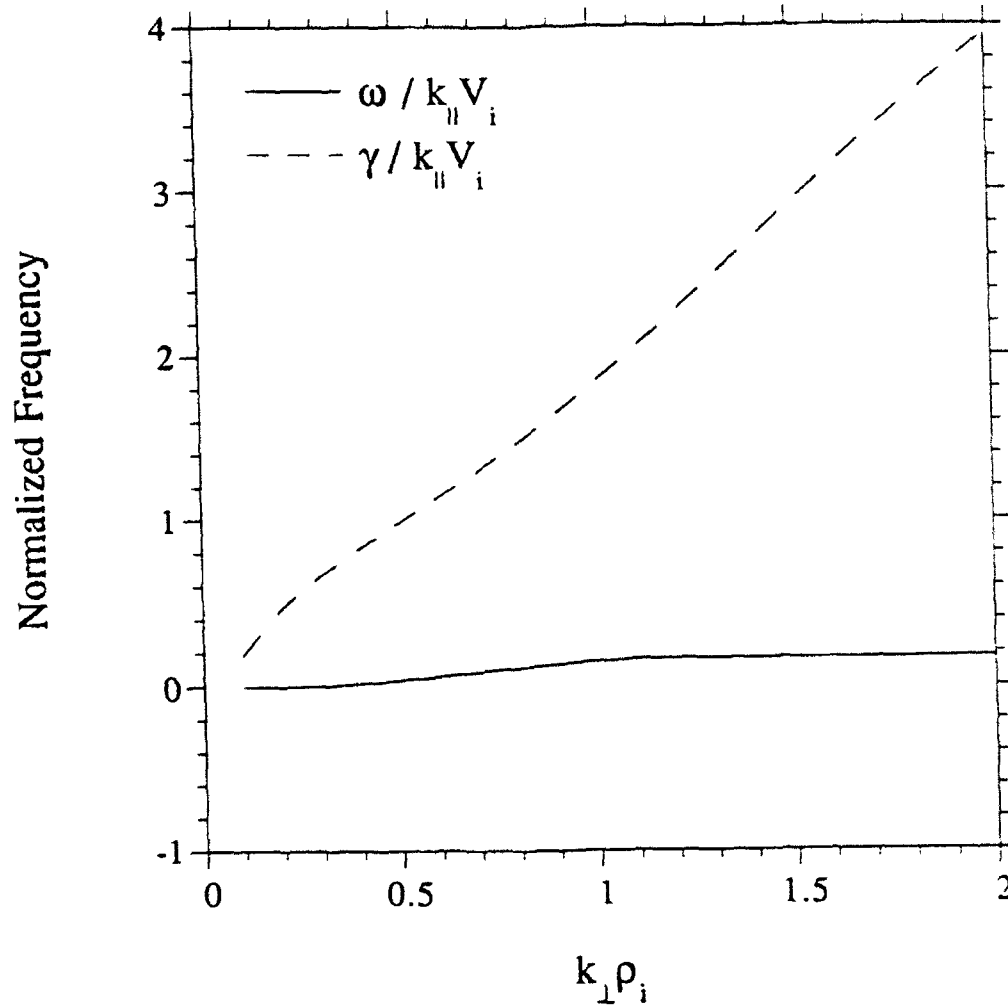Figure 28: Wave frequency and growth rate as a function of the ratio between perpendicular and parallel wave vectors for the drift mirror mode.

increasing $k_\perp \rho_i$.

The drift mirror mode, which is excited by temperature anisotropy, has the largest growth rate at small $k_\parallel/k_\perp$ (Figure 28). Figure 29 shows that the group velocity of the drift mirror mode has a wide range, varying from about 50 km/s at small $k_\parallel/k_\perp$ to zero when $k_\parallel/k_\perp$ is greater than 1. Therefore the drift mirror mode agrees well with the observed range of propagation velocity for stormtime Pc 5 waves, which varies from from 5 km/s to 40 km/s.

B.3   Low Phase Velocity Drfit Mode

The temperature gradient can also excite a low frequency wave mode with low phase velocity. This low phase velocity mode differs from the ion drift mode in having a transverse magnetic field component. For this mode, the value of transverse to compressional magnetic field amplitudes reaches as high as 0.6. whereas the ion drift mode is mainly compressional.

Figure 30 indicates that the instability of low phase velocity drift wave mode occurs for all values of $k_\perp \rho_i$. When $k_\perp \rho_i < 1$, the wave frequency is

Drift Mirror Mode
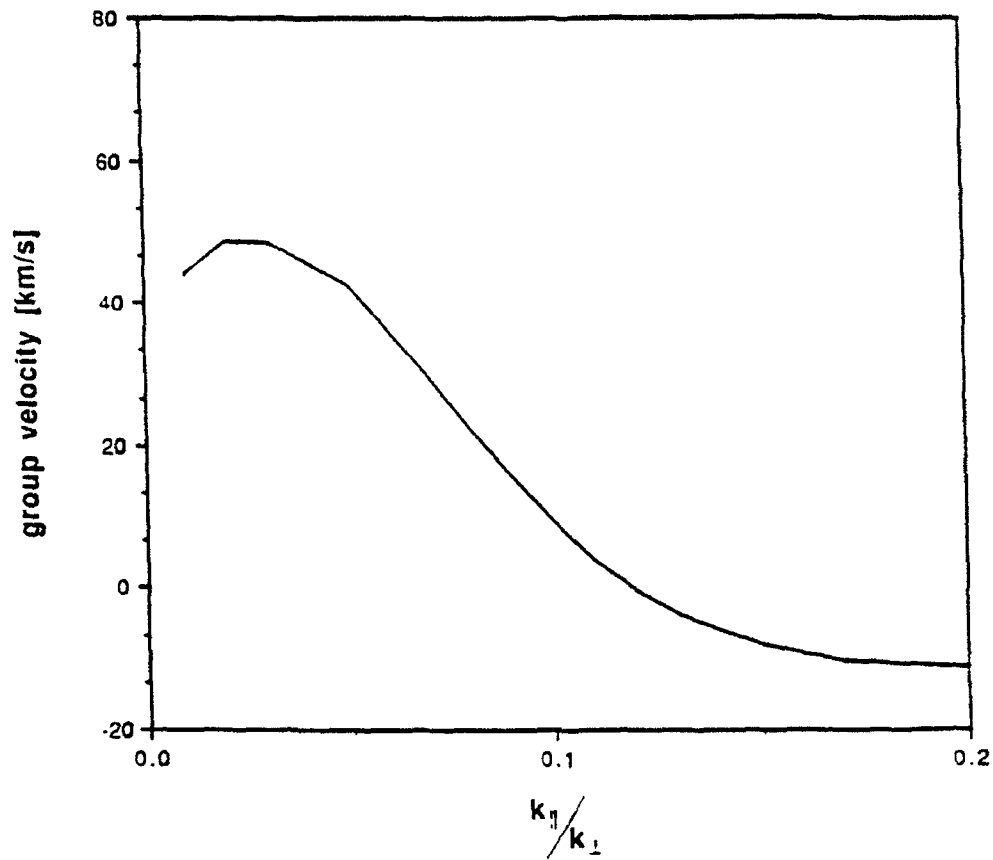
Figure 29: Perpendicular group velocity as a function of the ratio between perpendicular and parallel wave vectors for the drift mirror mode.

Low Phase Velocity Drift Mode
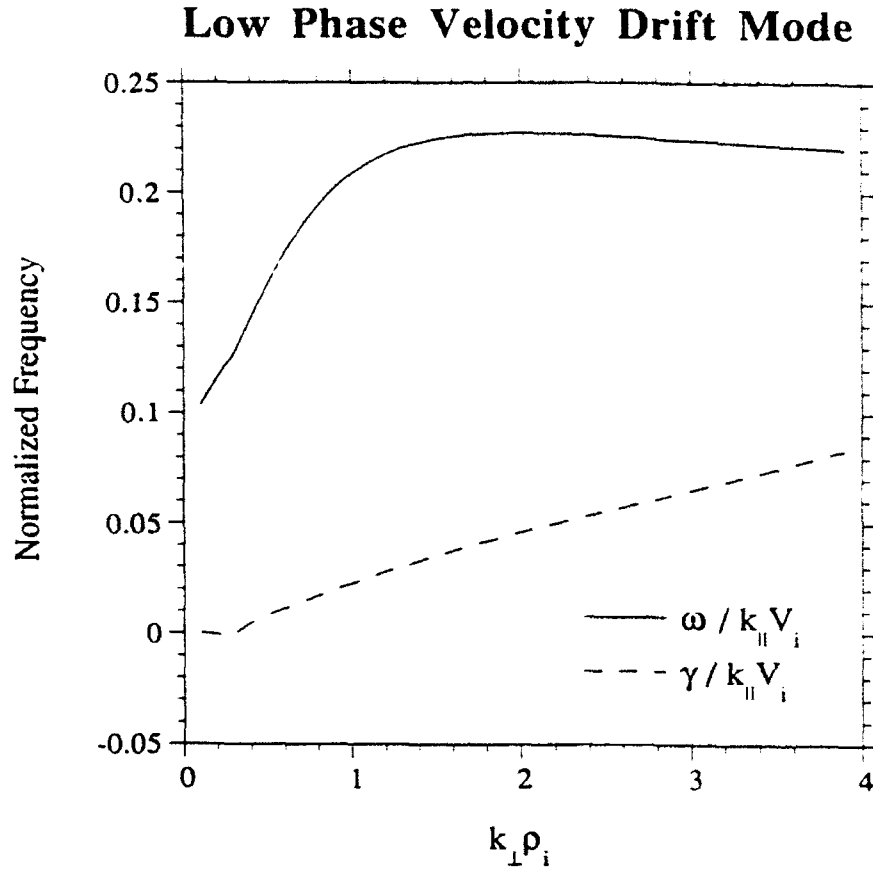
Figure 30: Wave frequency and growth rate as a function of the perpendicular wave vector for the low phase velocity drift mode.

positive. The wave frequency becomes negative as $k_\perp \rho_i$ increases above 1. Figure 31 shows that the group velocity for this low phase velocity mode is generally less than 10 km/s. Furthermore, the group velocity is positive only when $k_\perp \rho_i < 0.7$ (positive velocity corresponds to westward propagation in our geometry). Since storm time Pc 5 waves generally propagate westward with a velocity greater than 10 km/s, this wave mode cannot satisfactorily explain the GOES satellite observations.

Low Phase Velocity Drift Mode

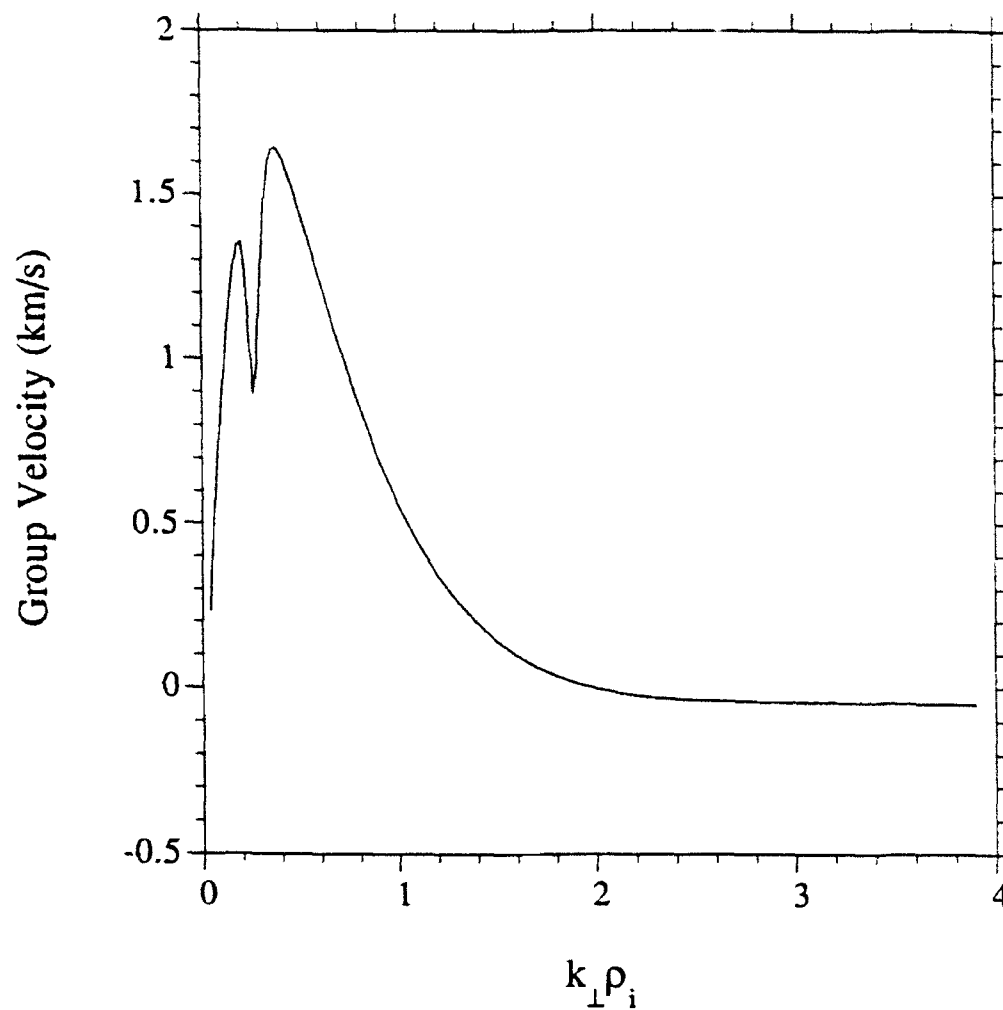

Figure 31: Perpendicular group velocity as a function of the perpendicular wave vector for the low phase velocity drift mode.

V Eigenmode Analysis of Low Frequency Waves in a Dipole Magnetic Field

A Eigenmode Equation

When the parallel wavelength is comparable to the curvature scale length, the local dispersion equation is no longer a good approximation. We therefore proceeded to solve an eigenmode equation of compressional waves in a dipole magnetic field. We used a gyrokinetic formalism to derive the eigenmode equation (Cheng and Lin, 1987)

$$\left\{ \vec{B} \cdot \nabla \frac{\sigma}{k_\perp^2 B^2} \vec{B} \cdot \nabla - \left[1 - \left(\frac{\omega}{k_\perp V_A}\right)^2 + \beta_\perp \left(1 - \frac{T_\perp}{T_\parallel}\right) \right] \right\} \tilde{B}_\parallel$$

$$-4\pi \int_T d^3v \frac{F_h}{T_\parallel} \frac{\omega - \omega_*^T}{\omega - \langle \omega_d \rangle} M^2 \mu^2 \left\{ \langle \tilde{B}_\parallel \rangle + \sum_{p=1}^{\infty} \frac{2\Gamma^2}{\Gamma^2 - p^2} \right.$$

$$\times [\cos(p\hat{\theta}) \langle \cos(p\hat{\theta}) \tilde{B}_\parallel \rangle + \sin(p\hat{\theta}) \langle \sin(p\hat{\theta}) \tilde{B}_\parallel \rangle]$$

$$\left. - \sum_{p=1}^{\infty} \frac{2p\Gamma(-1)^p \sin(\Gamma\hat{\theta})}{(\Gamma^2 - p^2)\cos(\pi\Gamma)} \langle \sin(p\hat{\theta}) \tilde{B}_\parallel \rangle \right\} = 0 \qquad (4)$$

Briefly we list the definitions in the equation:
(1) $\tilde{B}_\parallel$ is the parallel component of the complex wave field along ambient field $\vec{B}$ normalized by the magnitude of the equatorial ambient field.
(2) ω is the complex eigenfrequency.
(3) $\Gamma = (\omega - \langle \omega \rangle)/\omega_b$.
(4) $\langle \ldots \rangle$ denotes an averaging quantity along a trapped ion trajectory for a one bounce cycle.
(5) $\hat{\theta}$ is a function of polar angle and is expressed as an integral over a function of the ambient field.

The first two terms of Equation 4 give the conventional expression of compressional waves from magnetohydrodynamic (MHD) theory without kinetic effects. The integral contains the kinetic effects contributed by the trapped ions. This eigenmode equation, which can be solved for the eigenfunctions of $\tilde{B}_\parallel$ and the frequency ω, means physically that Pc 5 waves can be approximated as standing waves in the magnetosphere along ambient field lines. Overall, Equation 4 is an integro-differential equation that requires a five-dimensional integration (3 velocity integrations, 1 bounce average integration and the integration for $\hat{\theta}$). Furthermore, unlike the local dispersion equation, the frequency appears in a highly non-linear way through the function Γ. All this makes solving the equation computationally intensive. If we neglect the

last term with the integral $(-4\pi \int_T \cdots)$ which takes into account kinetic effects, the problem is simplified to the MHD case:

$$\left\{ \vec{B} \cdot \nabla \frac{\sigma}{k_\perp^2 B^2} \vec{B} \cdot \nabla - \left[1 - (\frac{\omega}{k_\perp V_A})^2 + \beta_\perp (1 - \frac{T_\perp}{T_\parallel}) \right] \right\} \tilde{B}_\parallel = 0 \qquad (5)$$

Our model uses a dipole magnetic field

$$\vec{B} = \frac{M}{r^3} (2 \sin \lambda \, \hat{r} - \cos \lambda \, \hat{\lambda}) \qquad (6)$$

On a given field line, $r = L \cos^2 \lambda$, and we introduce the variable $x = \sin \lambda$, so that our differential equation can be written as

$$q(x) \frac{d^2 b}{dx^2} + p(x) \frac{db}{dx} - [r(x) - \omega^2 s(x)] = 0, \qquad (7)$$

Here we have defined $b(x) = \tilde{B}_\parallel(\lambda)$. Other coefficients in Equation 7 are defined as:

$$
\begin{aligned}
q(x) &= \frac{\sigma}{(k_\perp L)^2 (1 + 3x^2)} \\
p(x) &= \frac{1}{(k_\perp L)^2 h(x) (1 + 3x^2)} \left[(\frac{d\sigma}{dh} h(x) + \sigma) \frac{dh}{dx} - \frac{3x\sigma h(x)}{1 + 3x^2} \right] \\
r(x) &= 1 + \beta_\perp (1 - \frac{T_\perp}{T_\parallel}) \\
s(x) &= \frac{\omega_{ci}^2}{(k_\perp V_A)^2}
\end{aligned}
$$

We also use the following definitions:

$$
\begin{aligned}
\sigma &= 1 + (\beta_\perp + \beta_\parallel)/2 \\
h(x) &= B_0 / B(x)
\end{aligned}
$$

$k_\perp$	perpendicular wave number
L	geosynchronous orbit radius ($\approx 6.6 R_E$)
$\beta_\parallel$	parallel fluid-to-magnetic pressure ratio
$\beta_\perp$	perpendicular fluid-to-magnetic pressure ratio
$T_\parallel$	parallel temperature
$T_\perp$	perpendicular temperature
ω_{ci}	ion cyclotron frequency

45

V_A Alfvén speed.

The boundary conditions are chosen at $x = 0$ and at $x = x_M$ such that

$$b(0) = 0$$

$$b(x_M) = 0$$

In the numerical solution we use $x_M = \sin 20°$.

To solve the equation we use the finite difference method. We solve for b values at N evenly-spaced points between 0 and x_M, so that $\Delta x = x_M/(N+1)$. Specifically, we approximate the derivatives at each point by central differences:

$$\left.\frac{db}{dx}\right|_i \longmapsto \frac{b_{i+1} - b_{i-1}}{2\Delta x}$$

$$\left.\frac{d^2b}{dx^2}\right|_i \longmapsto \frac{b_{i+1} - 2b_i + b_{i-1}}{(\Delta x)^2}$$

where the subscript i means the value at $x_i = i\Delta x$. We take the finite difference of Equation 7 at each point x_i to get a system of N equations in the $(N + 1)$ unknowns $b_1, \ldots, b_N, \omega$:

$$\left(\frac{q_i}{(\Delta x)^2} + \frac{p_i}{2\Delta x}\right) b_{i+1} + \left(-\frac{2q_i}{(\Delta x)^2} - r_i + \omega^2 s_i\right) b_i + \left(\frac{q_i}{(\Delta x)^2} - \frac{p_i}{2\mathcal{L}_r}\right) b_{i-1} = 0$$

for $i = 1, \ldots, N$ and where $b_0 = 0$ and $b_{N+1} = 0$ from our boundary conditions. In matrix notation we have

$$\mathbf{A}(\omega) \cdot \vec{b} = \vec{0} \tag{8}$$

in which $\mathbf{A}(\omega)$ is an $N \times N$ tridiagonal matrix. If $\vec{b}$ has nontrivial solutions, we obtain

$$\det[\mathbf{A}(\omega)] = 0. \tag{9}$$

We numerically solve this equation, using Newton method for solving the roots to obtain eigenfrequencies ω. For a particular solution ω, the system of equations is linear and homogeneous, so we expect to determine the eigenfunction up to a constant factor. We normalize our solutions by taking $b_1 = 1$. Using

this approach, we find a range of eigenfrequencies similar to those obtained by analytical solution of a local approximation to the MHD equation.

We next describe the evaluation of the kinetic term

$$K = -4\pi \int_T d^3v \frac{F_h}{T_{||}} \frac{\omega - \omega_*^T}{\omega - \langle \omega_d \rangle} M^2 \mu^2 \{\dots\}.$$

We first rewrite the integral, using the relation

$$\int_T d^3v \, f = \pi \int_0^\infty dv \, v^2 \int_{h_{min}}^h \frac{\frac{d\Lambda}{h}}{(1 - \frac{\Lambda}{h})^{1/2}} f,$$

where $\Lambda = h(x_T)$, h at the trapped-particle turning point. We next substitute the variables F_h and $T_{||}$ in terms of $\hat{v} = v/\bar{v}$, $A = (T_\perp/T_{||})_0$, and $\beta_{||}$ according to the following definitions:

$$F_h = \hat{v} \left(1 - \frac{T_{||}}{T_{\perp 0}} \Lambda\right)^{-3/2} (\pi \bar{v}^2)^{-3/2} e^{-\hat{v}^2}$$

$$\beta_{||} = \frac{8\pi \hat{v} T_{||}}{B_0^2} \left(\frac{T_\perp}{T_{||}}\right)_0$$

where the subscript 0 means to evaluate at zero latitude.

This substitution allows us to express the kinetic term in terms of known quantities. In the case of odd modes, when $\langle \tilde{B}_{||} \rangle = 0$, we express the kinetic term as

$$K(x; \omega, \tilde{B}_{||}) = -\int_r^{(x_T)^{max}} dx_T \int_0^\infty d\hat{v} \, C_1 \cdot \hat{v}^6 e^{-\hat{v}^2} \frac{\omega - \omega_*^T}{\omega - \langle \omega_d \rangle} \sum_{p=1}^\infty R_p \qquad (10)$$

where

$$C_1 = \frac{\beta_{||}}{2\sqrt{\pi}} (1 - \frac{T_{||}}{T_\perp})(1 - \frac{T_{||}}{T_\perp}\Lambda)^{-7/2} \frac{\Lambda^2}{h(x)} \frac{dh}{dx}(x_T)(1 - \frac{\Lambda}{h(x)})^{-1/2},$$

$$R_p = \frac{2\Gamma^2}{\Gamma^2 - p^2} \cos(p\hat{\theta})\langle\cos(p\hat{\theta})\tilde{B}_{||}\rangle$$

$$+ \frac{2\Gamma^2}{\Gamma^2 - p^2} \sin(p\hat{\theta})\langle\sin(p\hat{\theta})\tilde{B}_{||}\rangle$$

$$- \frac{2p\Gamma(-1)^p \sin(\Gamma\hat{\theta})}{(\Gamma^2 - p^2)\cos(\pi\Gamma)} \langle\sin(p\hat{\theta})\tilde{B}_{||}\rangle$$

$$\Gamma = \frac{\omega - \langle\omega_d\rangle}{\omega_b}$$

47

$$\hat{\theta} \;=\; \pi \frac{\int_{r=0}^{r=r} dl/v_{\parallel}}{\int_{r=0}^{r=r_T} dl/v_{\parallel}}$$

$$\text{and}\quad \omega_h \;=\; \frac{2\pi}{\tau_b}.$$

To derive the computational formulas in terms of x, we use the following definitions:

$$\vec{\kappa} \;=\; (\hat{\mathbf{e}}_b \cdot \nabla)\hat{\mathbf{e}}_b$$

$$\omega_B \;=\; \frac{cT_{\parallel}}{eB}\vec{k}_{\perp}\cdot\hat{\mathbf{e}}_b \times \nabla \ln B$$

$$\omega_{\kappa} \;=\; \frac{cT_{\parallel}}{eB}\vec{k}_{\perp}\cdot\hat{\mathbf{e}}_b \times \vec{\kappa}$$

$$\omega_{*} \;=\; \frac{cT_{\parallel}}{eB}\vec{k}_{\perp}\cdot\hat{\mathbf{e}}_b \times \nabla \ln n_h$$

$$\omega_d \;=\; \omega_B \frac{M\mu B}{T_{\parallel}} + \omega_{\kappa}\frac{Mv_{\parallel}^2}{T_{\parallel}}$$

$$\omega_{*}^{T} \;=\; \omega_{*}\frac{\partial \ln F_h}{\partial \ln n_h}$$

and the following relationships:

$$g(x) \;=\; \sqrt{\frac{h(x)[1+3x^2]}{h(x)-h(x_T)}}$$

$$G \;=\; \int_0^{x_T} g(x)\,dx$$

$$\tau_b \;=\; 4\frac{L}{v}G$$

$$\bar{v}^2 \;=\; \frac{2T_{\parallel}}{m(1-\frac{T_{\parallel}}{T_{\perp 0}}\Lambda)}$$

$$v_{\perp 0}^2 \;=\; \frac{2T_{\perp 0}}{m}$$

$$\omega_{ci} = \frac{eB}{m} \;=\; \frac{v_{\perp 0}}{\rho_0}$$

Using these definitions, we derive the variables in terms of x:

$$\hat{\theta}(x';x_T) \;=\; \pi\frac{1}{G}\int_0^{x'} g(x)\,dx$$

48

$$\langle \overline{\omega}_d \rangle = \hat{v}^2 \frac{1}{G} \int_0^{x_T} \overline{\Omega}_d \cdot g(x)\, dx$$

$$\overline{\Omega}_d = \overline{\omega}_\kappa \frac{2 - \frac{h(x_T)}{h(x)}}{1 - (1 - 1/A)\, h(x_T)}$$

$$\overline{\omega}_\kappa = -\frac{3}{2}\left(\frac{\rho_h}{L}\right)^2 \frac{mode}{A} \frac{1 - x^4}{(1 + 3x^2)^2}$$

$$\overline{\omega}_b = \hat{v} \cdot 2\pi \frac{\rho_h}{L} \frac{1}{G} \sqrt{\frac{1 - 1/A}{1 - (1 - 1/A)\, h(x_T)}}$$

$$\overline{\omega}_*^T = \frac{mode}{2A} \frac{\rho}{L} \left\{ \frac{\rho}{L_h} - 6\frac{\rho}{L} \frac{\left(\frac{A-1}{A}\right) x^2 (3 + 5x^2) h(x)}{\left(1 - h(x)\frac{A-1}{A}\right)(1 + 3x^2)^2} \right\}$$

where the over bar means that the frequency has been scaled by ω_{ci}, and L_h is the pressure gradient scale length. To compute the bounce averages of a variable f, we use the definition

$$\langle f \rangle = \frac{\int_{x=-x_T}^{x=x_T} (dl/v_\parallel) \cdot f}{\int_{x=-x_T}^{x=x_T} dl/v_\parallel}.$$

Since $\tilde{B}_\parallel$ is an odd function of x, $\cos(p\hat{\theta})\tilde{B}_\parallel$ is also, and we have

$$\langle \tilde{B}_\parallel \rangle = 0$$

$$\langle \cos(p\hat{\theta})\tilde{B}_\parallel \rangle = 0.$$

On the other hand, $\sin(p\hat{\theta})\tilde{B}_\parallel$ and ω_d are even functions of x, and we evaluate them using

$$\langle f \rangle = \frac{\int_{x=0}^{x=x_T} (dl/v_\parallel) \cdot f}{G}.$$

In evaluating the integral $\int (dl/v_\parallel)$ we encounter a singularity at $x = x_T$. Near this point we use an analytic function to approximate the integrand and integrate the approximation in closed form.

When computing $\langle \sin(p\hat{\theta})\tilde{B}_\parallel \rangle$ the period of $\sin(p\hat{\theta})$ may be on the order of the finite-difference spacing. To accurately evaluate the integral, we compute the integral over each subinterval from the known values of $\tilde{B}_\parallel$ and $(1/v_\parallel)(dl/dx)$ at each of the evenly-spaced points. We assume that these functions are linear over each subinterval, and we integrate, in closed form, $\sin(p\hat{\theta})\tilde{B}_\parallel(1/v_\parallel)(dl/dx)$. Then we simply sum these integrals over all subinter-

49

vals.

B Numerical Solutions

The procedure of solving the eigenmode equation is organized as follows: First, we solve the MHD case, as outlined above. The solution is then used as an initial guess in our iterative scheme. We proceed to solve for a new eigenfrequency, using the kinetic term computed from the MHD eigenfrequency and eigenfunction. Then we calculate a new eigenfunction, corresponding to the new eigenfrequency. This procedure is iterated until the estimated error is within acceptable bounds.

Soving the eiegnmode equation, we obtained the wave frequency and growth rate of the unstable eigenmode. Figure 32 plots the real and imaginary frequencies as a function of anisotropy. In addition, the growth rate solving from the MHD equation is also plotted in Figure 32 for comparison. In the MHD limit, the frequency of drift mirror waves is zero. Including the kinetic effects, the drift mirror mode has a small frequency, about 0.01 of the ion cyclotron frequency ($\omega/\omega_{ci} = 0.01$). More importantly, the eigenmode equatin indicates a smaller growth rate, in better agreement with the observations.

Figure 33 shows the eigenmode structure of magnetic field for the drift mirror mode versus θ for the parameters : $\beta_{\parallel} = 0.5, A = 2.2, L_h/\rho = -50, k_{\perp}L = 64, n_h/n_c = 0.1, L/\rho = 425, T_{\parallel}/T_c = 1000,$ and $L_h/L_b = -0.1$. This figure indicates that the wave amplitude reaches maximum at $\theta = 1°$ and decreases to zero when $\theta > 10°$. The wave amplitude of drift mirror waves is therefore localized near the equator. Since the wave amplitude vanishes near the equator, the wave has an odd mode structure with respect to the equator.
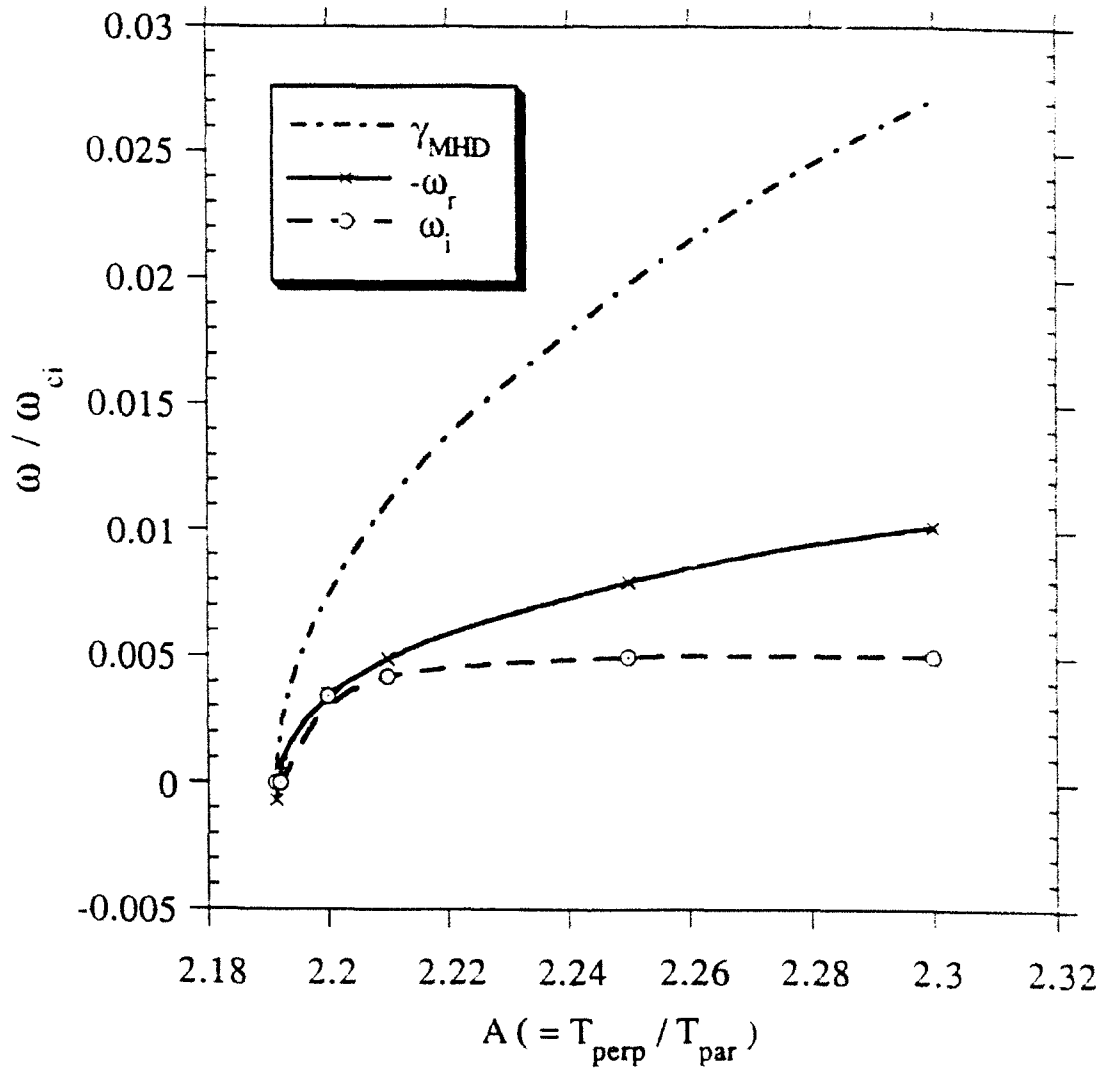
Drift Mirror Wave Instability

Figure 32: Wave frequency and growth rate as a function of anisotropy for the drift mirror mode
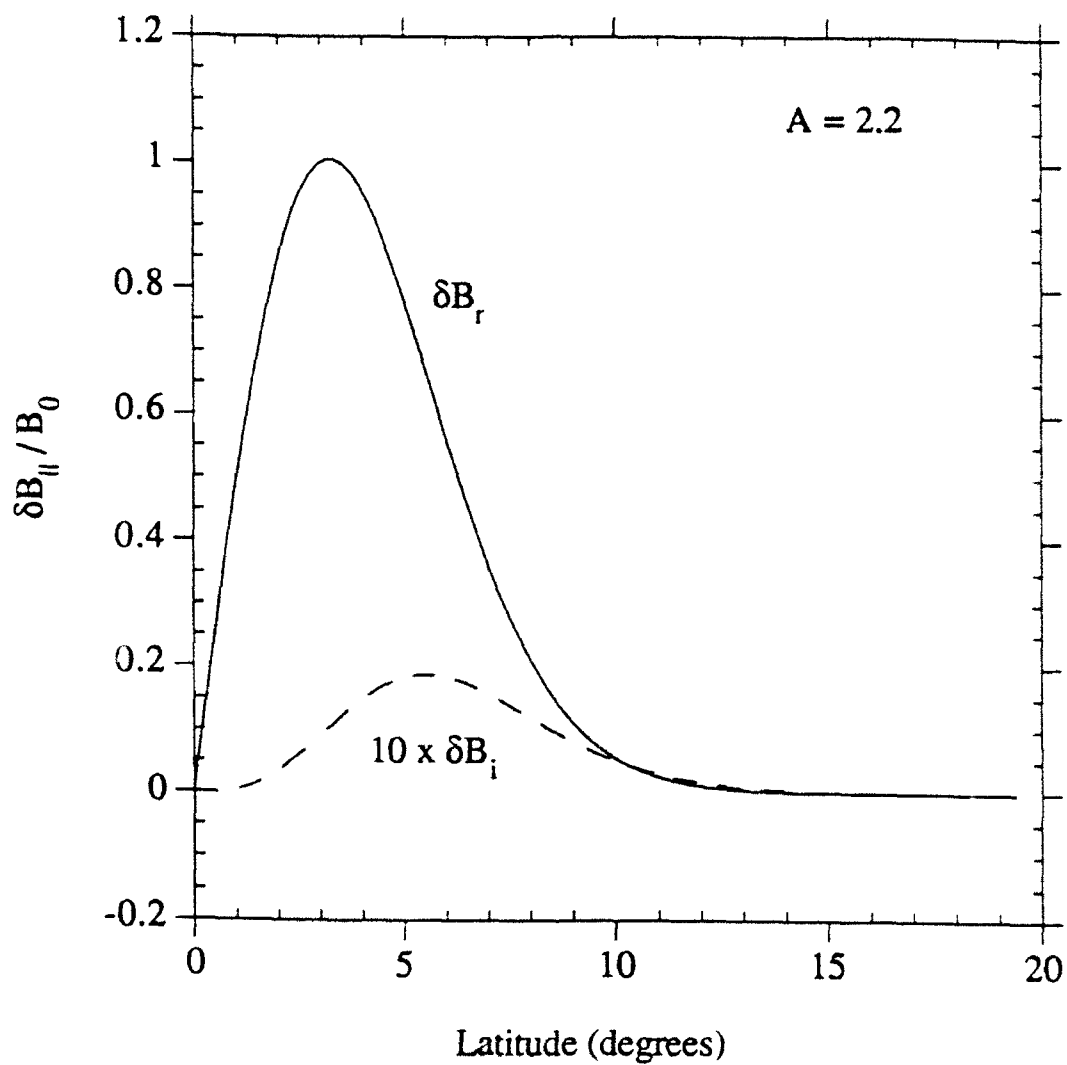
Eigenmode Structure

Figure 33: Eigenmode structure of magnetic field oscillations for the drift mirror mode. The y axis is the magnetic field wave amplitude normalized by magnetic field at the equator, and the x coordinate is the geomagnetic latitude.

VI Discussion

This project has demonstrated that stormtime Pc 5 waves observed by geostationary satellites in the afternoon sector are correlated with substorm onsets occurring near local midnight. The disturbed region of a stormtime Pc 5 event has a longitudinal extent varying between 30 and 90 degrees. The study shows that stormtime Pc 5 waves have a wave amplitude confined with about $10°$ from the magnetic equator. The propagation velocity of stormtime Pc 5 waves is typically about 15 km/s and can be as high as 45 km/s. The numerical solutions suggest that the propagation velocity of stormtime Pc 5 waves agrees better with the perpendicular group velocity of drift mirror mode.

The correlation between the occurrence of stormtime Pc 5 wave events and substorm onsets is not obvious because stormtime Pc 5 waves generally occur 2-4 hours after substorm onsets. Using the wave propagation velocity, we estimated the time for the wave to propagate from local midnight to the satellites. For the events studied. we were able to identify a substorm onset from ground magnetograms near local midnight within 20 minutes of the estimated times. Therefore, the results suggest that the occurrence of stormtime Pc 5 waves is correlated with substorm onsets. The correlation implies that stormtime Pc 5 waves are propagating westward with the substorm injected plasma. Since the propagation velocity is related to the energy of injected plasma, the larger propagation velocity would indicate that GOES satellites will encounter more energetic plasma as they move toward local midnight.

The correlation results depend on the accuracy in determining the wave propagation velocity. In order for GOES satllites to detect accurately the wave propagation velocity, the separation between the two GOES satellites needs to be less than 2 hours. We believe that the error in deducing the wave propagation speed is mainly caused by uncertainties in identifying the time of the first oscillation peak. which could at most have an error of one wave period. As Table 1 shows, the error in propagation speed is generally a few km/s when the propagation speed is greater than 10 km/s. This produces uncertainties in estimating the substorm onset times by about $\pm$ 20 minutes (Table 1). Since the actual substorm onsets generally occurred within 20 minutes of the estimated substorm onset time, the uncertainties in the propagation speed do not affect the qualitative conclusion that stormtime Pc 5 waves are related to substorm onsets.

In addition to uncertainties in propagation speed, other factors may affect the estimate of substorm onset times. For example, we have assumed a constant wave group velocity in the estimate. but the wave group velocity may vary with longitude and time, depending on the azimuthal variation of plasma parameters. Because the GOES 2 and 3 satellites at the geosynchronous orbit are separated only by two hours local time, the effects of the radial motion on estimating wave propagation speed should be small. Furthermore, since most stormtime Pc 5 waves occurred in the afternoon sector before dusk, the radial

motion of the injected plasma boundary may be unimportant for these events.

Another interesting observation is that the GOES 2 satellite often detected a stormtime Pc 5 event not observed by the GOES 5 satellite. This is peculiar because stormtime Pc 5 waves presumably propagate westward from GOES 5 to GOES 2. When GOES 5 did not observe the Pc 5 events, the magnetic field at GOES 5 had a large tail field. The explanation might be that the GOES 5 satellite was located at a higher magnetic latitude than GOES 2 and the waves were localized near the magnetic equator. This could also explain the observation that stormtime Pc 5 waves are not detected at large inclination angle (Baefield and Lin, 1983; Lin and Cheng, 1984).

The size of the region of stormtime Pc 5 waves has not been known before. The information about the size of disturbance region generally cannot be obtained from single satellite observations. By using dual satellite observations about the propagation velocity and event duration, we were able to estimate that the disturbed region of a stormtime Pc 5 event has a longitudinal extent varying between 30 and 90 degrees. The wave disturbance region in the evening hours is on the average smaller the disturbance region in the afternoon hours. The plasma clouds injected during substorms are responsible for exciting stormtime Pc 5 waves. As the substorm injected plasma cloud drifts westward, the front moves faster than the trailing edge. As a result, the plasma cloud expands.

The numerical solutions of the dispersion equation suggest that the propagation velocity of stormtime Pc 5 waves can be explained by the drift mirror mode (Section IV). The range of propagation velocity can be explained when the perpendicular wave vector times the ion gyroradius is less than 1 ($k_\perp \rho_i < 1$) and the parallel wave vector times ion gyroradius is in the range between 0.05 and 0.3 ($0.05 < k_\parallel \rho_i < 0.3$) (see Figure 25 and 27).

The correlation study indicates that the propagation velocity increases with wave frequency. Based on the numerical results, we argue that this correlation can be explained if parallel wavelength is the dominant parameter affecting the wave frequency of stormtime Pc 5 waves. Figures 24 and 25 indicate that both wave frequency and propagation velocity decrease with $k_\parallel \rho_i$. Therefore, propagation velocity would increase with wave frequency as parallel wavelength increases. The correlation between propagation velocity and wave frequency cannot be explained by varying perpendicular wavelength according to Figures 26 and 27. These two figures show that the perpendicular group velocity increases, whereas wave frequency decreases as $k_\perp \rho_i$ increases.

The correlation would also require that other parameters including perpendicular wavelength and plasma parameters do not vary much. This imply that the wave frequency of stormtime Pc 5 wave events is mainly determined by parallel wavelength. The eigenmode analysis presented in Section V has demonstrated that parallel wavelength of low frequency waves in a dipole filed is not an independent parameter. Parallel wavelength is an independent parameter only when the ambient magnetic field is straight. Parallel wavelength

is determined by the magnetic field configuration or magnetic field curvature.

The correlation study between wave frequency and magnetic field properties supports the eigenmode analysis. Since wave frequency of stormtime Pc 5 waves is also correlated with the inclination angle (Figures 17 and 18), parallel wavelength is in turn determined by the inclination angle or the magnetic field topology. A magnetic field configuration with a large tail field during magnetic storms will have a large inclination angle or a large magnetic field curvature. For such a magnetic field configuration, stormtime Pc 5 waves would have a higher wave frequency.

In summary, the propagation velocity of stormtime Pc 5 waves is consistent with the perpendicular group velocity of drift mirror mode. The propagation velocity increases with wave frequency and the magnetic field inclination angle. The wave frequency of stormtime Pc 5 waves appears to be mainly determined by wave parallel wavelength, which is in turn determined by the inclination angle or the magnetic field topology.

Finally the present study suggests that remote diagnosis of substorm activities from dayside snchronous satellites is feasible. The onset of stormtime Pc 5 waves observed in the dayside can be used to help specify the nightside ionospheric condition, and the disturbed environment at the synchronous orbit. In principle, it is feasible to use real time observations of magnetic pulsations to diagnose remotely the plasma environment that a synchronous satellite is about to go through during substorms. For example, a fast moving stormtime Pc 5 event indicates that the magnetic field configuration ahead in the evening sector is stretched tailward. Therefore, more substorm injections are likely. On the other hand, a slow moving stormtime Pc 5 event might indicate a more relaxed magnetic field configuration. Thus substorm activity is subsided. The observations of low frequency magnetic pulsations might be useful for planning synchronous satellite operations

VII References

Allan, W., E. M. Poulter, and E. Nielsen, STARE observations of a Pc 5 pulsation with large azimuthal wave number, *J. Geophys. Res.*, *87*, 6163, 1982.

Barfield, J. N., and P. J. Coleman, Jr., Storm-related wave phenomena observed at the synchronous equatorial orbit, *J. Geophys. Res.*, *75*, 1943, 1970.

Barfield, J. N., and C. S. Lin, Remote determination of the outer radial limit of stormtime Pc 5 wave occurrence using geosynchronous satellites, *Geophys. Res. Lett.*, *10*, 671, 1983.

Barfield J. N., R. L. McPherron, P. J. Coleman, Jr., and D. J. Southwood, Storm-associated Pc 5 micropulsation events observed at the synchronous equatorial orbit, *J. Geophys. Res.*, *77*, 143, 1972.

Barfield, J. N., and R. L. McPherron, Statistical characteristics of storm-associated Pc 5 micropulsations observed at the synchronous equatorial orbit, *J. Geophys. Res.*, *77*, 4720, 1972.

Cheng, C. Z., and C. S. Lin, Eigenmode analysis of compressional waves in the magentosphere, *Ceophys. Res. lett.*, *14*, 884, 1987.

Hasegawa, A., Drift mirror instability at the magnetosphere, *Phys. Fluids.*, *12*, 2642, 1969.

Lanzerotti, L. J., C. G. Maclennan, H. Fukunishi, J. K. Walker, and D. J. Williams, Latitude and longitude dependence of storm time Pc 5 type plasma waves, *J. Geophys. Res.*, *80*, 1014, 1975.

Lin, C. S., and J. N. Barfield, Azimuthal propagation of storm time Pc 5 waves observed simultaneously by geostationary satellites GOES 2 and GOES 3, *J. Geophys. Res.*, *90*, 11,075 1985.

Lin, C. S., and C. Z. Cheng, Tail field effects on drift mirror instability, *J. Geophys. Res.*, *89*, 10771, 1984.

Lin, C. S., J. Koga, and H. D. Ling, A study of propagation velocity of storm-time Pc 5 waves at synchronous orbit, EOS, 73, 249, 1992.

McIlwain, C. E., Substorm injection boundaries, in *Magnetospheric Physics*, edited by B. M. McCormac, p. 143, D. Reidel, Hingham, Mass., 1974.

Moore, T. E., R. L. Arnoldy, J. Feynman, and D. A. Hardy, Propagating substorm injection fronts, *J. Geophys. Res.*, *86*, 6713, 1981.

Mauk, B. H., and C. E. McIlwain, Correlation of Kp with the substorm injected plasma boundary, *J. Geophys. Res.*, *79*, 3193, 1974.

Ng, P. H., and V. L. Patel, The coupling of shear Alfven and compressional waves in high-β magnetospheric plasma, *J. Geophys. Res.*, *88*, 10035, 1983.

Pangia, M. J., C. S. Lin, and J. N. Barfield, A correlative study of Pc 5 magnetic pulsations with substorm onsets, J. Geophys. res., 95, 10699, 1990.

Takahashi, K., P. R. Higbie, and D. N. Baker, Azimuthal propagation and frequency characteristics of compressional Pc 5 waves observed at geosta-

tionary orbit, *J. Geophys. Res.*, *90*, 1473, 1985.

Walker, A. D. M., B. A. Greenwald, A. Korth, and G. Kremser, STARE and GOES 2 observation of a storm time Pc 5 ULF pulsation, *J. Geophys. Res.*, *87*, 9135, 1982.

Appendix

List of Stormtime Pc 5 Events

List of Stormtime Pc 5 Wave Events in 1979 - 1980

No.	Date	Start Time (HH:MM)	Time Delay (min)	Wave period (min)	Velocity (km/s)
1	3/25/79	21:38	38	4.5	6.67
2	3/28/79	20:18	31	9.25	8.87
3	3/28/79	22:28	26	3.0	11.17
4	3/28/79	23:08	34	2.75	7.82
5	3/29/79	18:00	17	6.8	18.72
6	4/01/79	17:18	30	7.4	9.27
7	4/02/79	16:48	43	9.5	5.53
8	4/21/79	21:37	31	3.8	8.87
9	9/20/79	19:24	10	6.1	34.61
10	9/21/79	0:36	7	2.4	50.59
11	9/26/79	1:24	15	2.8	21.80
12	9/26/79	20:04	17	4.8	18.87
13	9/29/79	0:10	28	3.5	10.24
14	10/8/79	23:38	9	3.0	37.98
15	10/12/79	23:06	24	4.4	12.21
16	11/13/79	20:03	19	5.4	15.32
17	11/15/79	18:35	11	9.2	28.82
18	11/24/79	21:42	14	4.0	22.07
19	1/1/80	19:03	42	5.6	4.94
20	1/1/80	21:42	25	4.4	10.41
21	1/13/80	18:54	25	6.0	10.31
22	1/13/80	22:03	21	3.5	12.86
23	1/14/80	1:18	20	4.4	13.60
24	2/16/80	19:34	37	6.0	5.66

* Event date and start time were based on GOES 2 observations.
* time delay is measured from the wave onset time at GOES 2 to the wave onset time at GOES 3.

List of Stormtime Pc 5 Wave Events in 1983

No.	Date	Start Time (HH:MM)	Time Delay (min)	Wave period (min)	Velocity (km/s)
1	1/14/83	23:59	25	3.1	13.52
2	1/15/83	01:51.5	21.5	2.8	16.23
3	1/17/83	23:21	12	2.8	31.52
4	1/24/83	22:46.5	13	3.0	28.86
5	2/11/83	20:25	13	3.6	28.38
6	2/20/83	19:44	57.5	3.4	3.98
7	3/5/83	22:13	21	4.0	16.10
8	3/12/83	18:26	41	4.0	6.71
9	3/18/83	22:22.5	19.5	3.2	17.70
10	3/25/83	20:03	39	12	7.31
11	3/28/83	17:19.5	10	4.0	37.58
12	3/28/83	19:15	9	4.6	42.10
13	4/14/83	20:12	10.5	3.0	35.64
14	4/14/83	23:44.5	15.9	4.3	22.49
15	4/24/83	23:07.5	10.5	3.2	35.52
17	4/30/83	21:35	17	2.6	20.61
18	9/19/83	1:03	22	2.4	30.40
19	10/14/83	1:24	26	2.5	25.53
20	10/18/83	20:06	24	2.7	28.02
21	10/24/83	0:18	20	2.9	34.36
23	11/12/83	20:28	34	4.5	19.12
24	11/15/83	12:29	-28	2.9	-30.02
25	11/25/83	22:33	41	3.2	14.94
26	12/5/83	22:19	48	3.2	12.23
27	12/31/83	23:00	22	3.3	31.02
28	3/1/83	0:13	28	2.4	11.30
29	3/2/83	14:36	57	5.8	3.98
30	3/12/83	20:07	62	6.0	3.39
31	3/28/83	21:07	48	4.4	5.38

* Event date and start time were based on GOES 5 observations.
* time delay is measured from the wave onset time at GOES 5 to the wave onset time at GOES 2.

List of Stormtime Pc 5 Wave Events in 1986

No.	Date	Start Time (HH:MM)	Time Delay (min)	Wave period (min)	Velocity (km/s)
1	1/6/86	20:59	47	4.0	5.67
2	1/9/86	22:00	25	3.0	13.47
3	1/21/86	22:11	56	3.4	4.37
4	1/25/86	3:24	15	8.5	24.85
5	2/11/86	4:10	32	2.7	10.04
6	2/21/86	23:06	13	3.0	29.14
7	3/7/86	20:31	15	3.2	24.35
8	3/25/86	22:16	15	3.6	23.03
9	3/6/86	20:05	59	8.3	3.91
10	3/6/86	22:13	33	5.0	9.42
11	8/29/86	23:01	11	2.5	24.33
12	9/23/86	21:21.5	14.5	3.2	17.03
13	10/18/86	20:17.5	16.5	4.5	13.47
14	11/4/86	16:54	13	5.3	17.64
15	11/15/86	1:46	16	2.8	14.29
17	11/24/86	20:29	8	3.2	34.61
18	12/21/86	22:58	12	3.2	30.70
19	12/23/86	21:53	18	3.2	19.43
20	1/18/86	0:42	16	2.8	23.02

* Event date and start time were based on GOES 5 observations.
* time delay is measured from the wave onset time at GOES 5 to the wave onset time at GOES 6.